KU ScholarWorks

Opposites Attract: Synthesis and Electrochemical Studies of Electron-Rich and Electron-Poor Rhodium Complexes for Hydrogen Evolution Catalysis

Item Type	Undergraduate research project
Authors	Henke, Wade C.
Publisher	Department of Chemistry, University of Kansas
Rights	Copyright 2017 Wade C. Henke
Download date	2024-08-26 22:15:11
Link to Item	https://hdl.handle.net/1808/26441

Opposites Attract:
Synthesis and Electrochemical Studies of Electron-Rich and Electron-Poor Rhodium Complexes for Hydrogen Evolution Catalysis

Thesis by
Wade C. Henke

In Partial Fulfillment of the Requirements for the Degree of
Bachelor of Science with Honors in Chemistry

Lawrence, Kansas
May 2017

© 2017

Wade C. Henke

All Rights Reserved

Acknowledgments

I would like to express my profound appreciation and thankfulness to James D. Blakemore for allowing me to join his research group and mentoring me. I think a lot about the day James asked me, “What are your plans for the summer?” That was the day I asked if he was looking for any undergraduate students to work in his lab, and I went home that night with the task of finding a substituted bipyridine synthesis. James personally taught me how to use each piece of equipment in the laboratory, from the Schlenk line to the glovebox. He was also in the lab to show me how to run my first few syntheses. Today, if I asked James if I could make any more substituted bipyridines I think he would disown me. I have never had a mentor that was so supporting, so willing, and so eager to teach me about chemistry. James, I will be forever grateful that you allowed me to be a part of your lab and I will never forget that you encouraged me to pursue departmental honors and graduate school. Graduate school wouldn’t have been on my radar if it wasn’t for you. I am excited to attend graduate school at the University of Kansas to continue my work under your mentorship. For all the opportunities you have presented me in the last year, thank you.

I would also like to express my gratitude to Davide Lionetti, our postdoctoral synthetic genius. Thank you for continually answering my questions, teaching me about synthesis, group theory, and X-ray crystallography. I remember the day I asked you, “why is aqua regia red?” Then you told me to go to the whiteboard and draw the molecular orbital diagram for NO_2. I appreciate that you always answer my questions, but that you don’t

directly give me the answer at first. Rather, you guide me, and teach me about what I ask through chemical principles. Thank you for your guidance and expertise.

I have had an excellent experience working with each of the members of the Blakemore group. Will Moore, thank you for all your hard work in the lab, willingness to learn new techniques, and synthetic output. I have learned a lot from you, enjoy seeing your synthetic knowledge grow, and look forward to continue working with you as your mentor. David Sconyers, thank you for answering my questions, teaching and working with me on electrochemistry. Yun Peng, thank you for teaching me how to use the gloveboxes and about my hairstyle. Tyler Kerr, thank you for always talking with me, letting me bounce ideas off you, and teaching me how to do day-to-day tasks around the lab. Keaton Prather, thank you as well for talking with me, letting me bounce ideas off you, and teaching me several bipyridine syntheses. Julie Hopkins, thank you for showing me how to avoid liquid oxygen and how to properly set up the vacuum traps for the box. Emily Boyd, Katie Cannon, and Amit Kumar, thank you for your tremendous support, help, and feedback. It has been a pleasure to work with everyone in the Blakemore group and I look forward to continue working with you.

Thank you to Victor Day, our talented X-ray crystallographer, for teaching and working with me on crystal structures. Thank you to Sarah Neuenswander, for your help and teaching me how to use the NMR.

I would like to extend a special thank you to J.P. Matheny for being the teaching assistant that inspired me to be a chemist. J.P. thank you for answering my questions and giving me the opportunity to get involved in research early on at KU. Also, thank you to Michael Rubin for being my first P.I. and Andy Edwards for being my first graduate student guide.

To my thesis committee: Dr. Benson, thank you for your support and teaching during my three years at KU. Your organic chemistry class specifically, is what encouraged me to become a chemistry major. Dr. Elles, thank you for your support and your ability to take a complicated subject like physical chemistry and explain it in a way that truly makes me excited about chemistry and the world around us. You are an educator first, and this means a lot to me as a student at a large research university. Dr. Jackson, thank you for your support and thank you for being an excellent educator. Your special topics course is what got me interested in inorganic chemistry and the world of transition metals.

Deanne Arensberg, thank you for being my mom away from my mom. You have helped me more than I could ever express. If I ever had a question or doubt I knew that I could come talk to you and the issue would be resolved. I will never forget when you invited a group of us over to have dinner at your home. A home cooked dinner before finals is difficult to come by, especially one so delicious. You are absolutely awesome and I will always appreciate everything you have done for me while at KU.

I would like to thank, my mom, my dad, and my grandmother. Mom, Dad, and Mamama, thank you for your tremendous support through my undergraduate career. Mom, thank you for always being there, listening, and letting me talk things through with you. Dad, I hope you know that I always remember you saying, “school gets harder every year.” School does get harder, each semester, even, but you, mom, and Mamama are the best support system in the world. Mamama, thank you for always listening to me talk about chemistry and always being such a positive influence in my life. I could have an awful week, but if I got the chance to talk to you on the weekend I was always ready for the next week after one of your pep talks. Thank you, mom, dad, and Mamama for your unconditional positive regard and I love you all.

Lastly, I would like to thank you, Maddie, for continually showing me support as I continue to pursue chemistry. You are my best friend and I am so happy that we have gotten to experience all that college has to offer, together. Good news, or bad news, you are always the first person I turn to and your unwavering support and encouragement has meant more to me than words can express; you are truly my rock (cliché, yes, but so very true). Maddie, if it wasn’t for you I would not be where I am today. I definitely wouldn’t be graduating with a bachelor of science, and I would probably still be stuck somewhere, pursuing something insignificant. I am the happiest I have ever been, and I will be forever grateful to you for encouraging me to always pursue education. I am excited for what the future has in store for us and I love you always ❤️.

Abstract

Electrocatalysis represents an attractive route to coupling renewable energy sources such as wind or solar power with sustainable generation of chemicals. An attractive target chemical would be hydrogen gas because it can be used as a fuel that does not emit pollution (CO_2). Progress toward this goal is hampered by a poor mechanistic understanding of how the electrocatalysts couple electrons with substrates to generate products. This problem is especially serious in the case of highly active catalysts that involve redox-active or proton-responsive ligands. Rhodium compounds featuring pentamethylcyclopentadienyl (Cp*) and diimine-type ligands are especially complex because they involve both of these modes of non-innocence. Changes in ligand substitution patterns are often used to improve the activity and stability of catalysts, but the consequences of such modifications are unknown in this class of catalysts. This limits the usefulness of these compounds and their incorporation into more elaborate energy-conversion systems. Here, we will discuss two specific cases that involve use of electron-donating and electron-withdrawing bipyridine variants.

Specifically, this thesis describes the synthesis and electrochemical properties of two novel rhodium compounds featuring pentamethylcyclopentadienyl (Cp*) and 4,4′-disubstituted 2,2′-bipyridine (bpy) ligands. The compounds were prepared with two disubstituted bipyridine derivatives, 4,4′-bis(*tert*-butyl)-2,2′-bipyridine (tBu-bpy) and 4,4′-bis(trifluoromethyl)-2,2′-bipyridine (CF_3-bpy); these ligands are more electron-donating and electron-withdrawing, respectively, than the parent underivatized bpy system. Once synthesized these compounds were characterized using ^{1}H, $^{13}C\{^{1}H\}$, and $^{31}P\{^{1}H\}$ nuclear magnetic resonance, mass spectrometry, UV-visible spectroscopy and single-crystal X-ray diffraction.

Electrochemical studies with these complexes revealed that they are catalysts for hydrogen production. The catalytic activity is modulated by the choice of ligand. Compared to the parent bpy complex, the overpotential for hydrogen evolution is shifted to a smaller value for the $[Cp^*Rh(CF_3\text{-bpy})Cl]^{+}(PF_6)^{-}$ complex, but shifted to a larger value for $[Cp^*Rh(tBu\text{-bpy})Cl]^{+}(PF_6)^{-}$. Bulk electrolyses carried out with these complexes confirmed catalytic turnover and a high faradaic efficiency for hydrogen evolution in all

cases. Notably, $[(Cp^*H)Rh(CF_3\text{-bpy})NCMe]^+$, a putative intermediate in the process of hydrogen evolution, was detected by ^1H NMR following electrocatalytic H_2 generation with $[Cp^*Rh(CF_3\text{-bpy})Cl]^+(PF_6)^-$. Few such $[(Cp^*H)Rh]$ complexes have been observed or reported in past work, and the observation of a species of this type therefore suggests a general role for such intermediates in hydrogen evolution with this class of catalysts.

Table of Contents

List of Figures and Schemes

Figures *Pages*

Figures (continued) *Pages*

Schemes....*Pages*

List of Equations and Tables

Equations *Pages*

Table Page

Nomenclature

1. $[Cp^*Rh(tBu\text{-}bpy)Cl]^+(PF_6)^-$

2. $[Cp^*Rh(bpy)Cl]^+(PF_6)^-$

3. $[Cp^*Rh(CF_3\text{-}bpy)Cl]^+(PF_6)^-$

BPG. Basal plane of highly oriented pyrolytic graphite

Bpy. 2,2′-bipyridyl

CV. Cyclic voltammetry

Cp*. 1,2,3,4,5-pentamethylcyclopentadienyl

DMF: Dimethylformamide

Fc. Ferrocene

Fc^+. Ferrocenium

CF_3-bpy. 4,4′-trifluoromethyl-2,2′-bipyridine

GC. Gas chromatography

HSQC. Heteronuclear single quantum coherence spectroscopy

J. Coupling Constant

L. Ligand

MeCN. Acetonitrile

NMR. Nuclear magnetic resonance

tBu-bpy. 4,4′-*tert*-butyl-2,2′-bipyridine

THF. Tetrahydrofuran

UV-Vis. UV-Visible (Electronic Absorption) spectroscopy

XRD. X-ray diffraction

Chapter 1

SYNTHESIS AND CHARACTERIZATION OF NOVEL RHODIUM COMPOUNDS FEATURING NON-INNOCENT LIGANDS

Introduction

Society's rapid consumption of available fuel sources will eventually leave those who inhabit the Earth starved for easily accessible energy and fuel. Although wind, geothermal, and hydroelectric power systems are beneficial, they do not represent a way to effectively produce energy for long-term use. The sunlight that hits the Earth everyday provides more energy in one hour than humans could use in an entire year.[1] However, due to the inhomogeneous nature of solar illumination, storage and transport of captured energy would be necessary for adequate supply at the point of use. One possible solution to this problem is the storage of energy produced from renewable resources (e.g. solar) into chemical bonds. Electrons can be harvested and replenished, using renewable energy, in a catalytic cycle capable of producing useful chemicals and fuels. This would provide an on-demand supply of energy, with accessibility that would support human consumption well into the future. An attractive route to producing clean and renewable energy would be to use a catalyst to split water (producing dioxygen, O_2) and couple the resulting protons and electrons to produce hydrogen gas (H_2), resulting in an energy source with little environmental impact.

$$2H_2O \rightleftharpoons O_2 + 4H^+ + 4e^- \quad E^0 = 1.23V \quad (1.1)$$

$$4H^+ + 4e^- \rightleftharpoons 2H_2 \quad E^0 = 0.00V \quad (1.2)$$

$$2H_2O \rightleftharpoons O_2 + 2H_2 \quad E^0 = 1.23V \quad (1.3)$$

Water splitting is composed of two half reactions, as shown in the above equations (1.1-1.3).[2] Hydrogen evolution catalysis represents a reaction pathway where we can take these protons and electrons from this water splitting reaction and turn them into H_2 as a sustainable fuel.

A catalyst previously reported by Grätzel and co-workers bears an η^5-pentamethylcyclopentadienyl (Cp*) ligand, a chelating κ^2- 2,2′-bipyridine (bpy), and a proposed hydride attached to a rhodium metal-center (see Figure 1.1).[3]

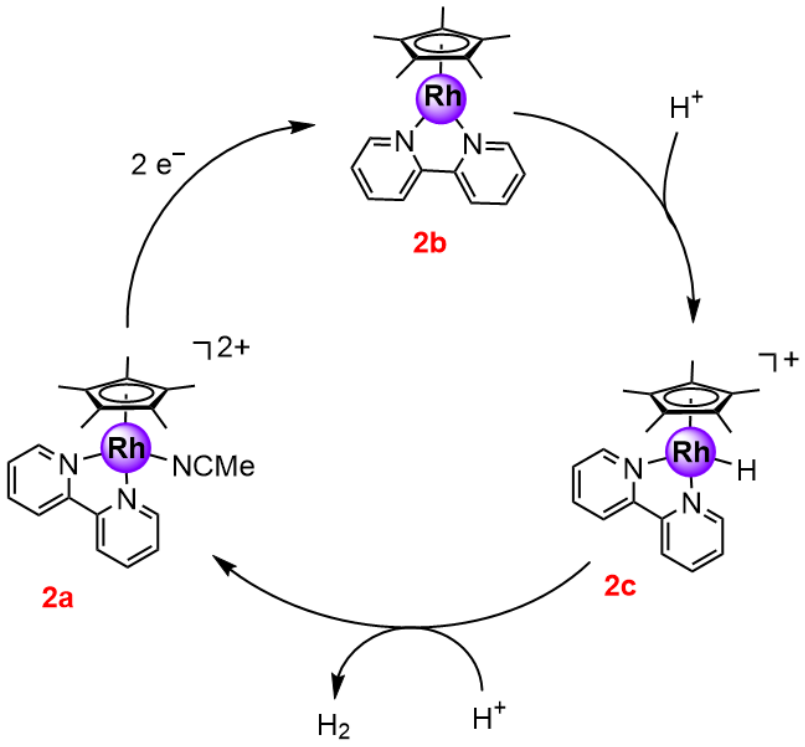

Figure 1.1: Hydrogen evolution pathway by Grätzel and co-workers; describing the route to hydrogen evolution with rhodium complexes of this type.

The starting 18e⁻, six-coordinate [Rh^{III}] complex, is reduced by 2e⁻ to obtain the 18e⁻, five-coordinate, [Rh^{I}] complex. Addition of an acid source then forms a purported [Rh^{III}]

hydride. This metal hydride is believed to be the reactive intermediate, highlighting a step in the mechanism for hydrogen evolution for this class of catalysts.[3]

In 1993, Chardon-Noblat et al. studied the electrochemical properties of **2a.** They reconfirmed Grätzel's results and were able to identify **2b** via electrochemical methods. They then immobilized **2a** using a covalent-polymeric film and were able to demonstrate the electrocatalytic ability of these [Rh] complexes for hydrogen evolution.[4]

In 2005, the Pandey group also synthesized **2a** in order to understand the role of solvent in ligand substitution reactions. Different solvent polarities (benzene to methanol) were used to demonstrate that substitution patterns around the metal center could be controlled and result in a complex with the desired substituted ligand.[5]

In 2013, the Gray group was able to non-covalently immobilize a [Rh] catalyst, similar to **2a**, using a pyrene appended 4,4′-disubstituted bipyridine. The pi stacking from the pyrene groups allowed for the catalyst to be attached to the surface of a carbon electrode. X-ray photoelectron spectroscopy of an electrode soaked in a solution of the pyrene appended [Rh] complex confirmed the immobilization of the catalyst. After soaking and rinsing the electrode, a bulk electrolysis was performed and the resulting head space of the electrolysis cell was sampled and analyzed by gas chromatography, which confirmed catalytic hydrogen evolution.[6]

In 2014, Blakemore et al. reported the synthesis of a variety of pentamethylcyclopentadienyl complexes bearing bipyridine (**2a**) and 1,10-phenanthroline ligands in Rh^{III} and Rh^{I} oxidation states. A crystal of **2b** was obtained–the first time a crystal structure of **2b** had been obtained. This study was used to better understand the

electronic structure of these [Rh] complexes and to synthesize a variety of useful analogues of the parent catalyst described by Grätzel.[7]

Recently, Blakemore and co-workers reported that addition of weak acid to compound **2b** above does not result in formation of a detectable hydride species, by ^{1}H NMR, but rather identified formation of another rhodium species, bearing an η^4-pentamethylcyclopentadiene (Cp*H) ligand. Addition of stronger acid to this [(Cp*H)Rh] compound results in formation of hydrogen gas with unity yield. Thus, this unusual compound is an active intermediate en route to hydrogen evolution (see Figure 1.2).[8]

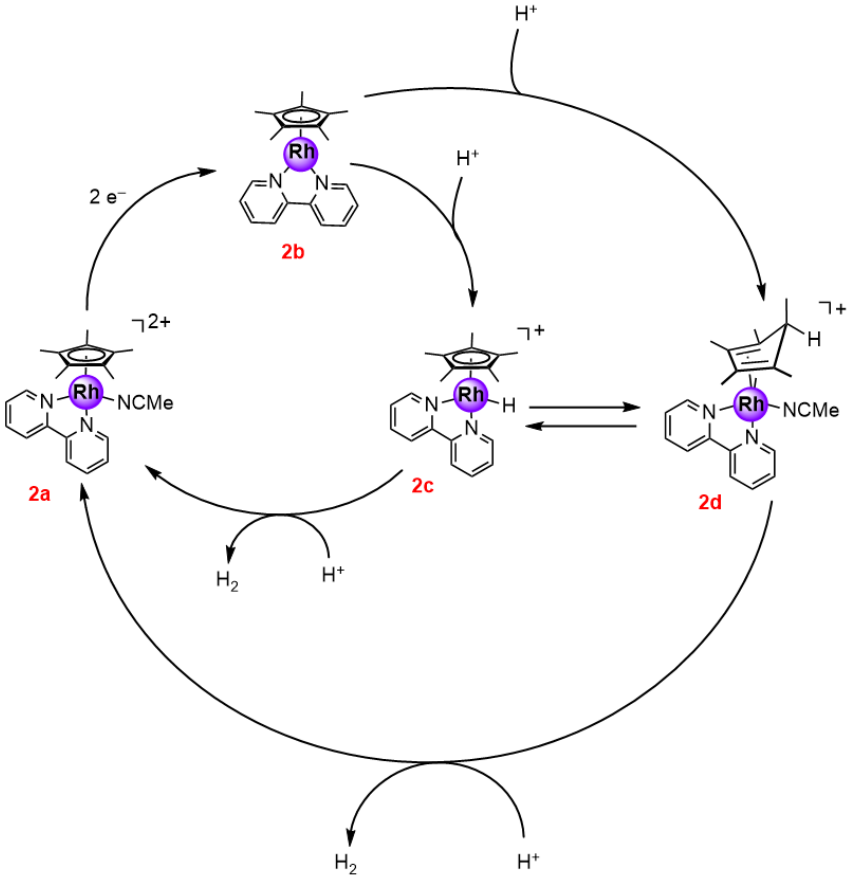

Figure 1.2: Hydrogen evolution pathway by Blakemore and co-workers; highlighting the formation of Cp*H as a pathway to hydrogen evolution.

The Cp* ring, initially a pi donor, becomes a pi-acceptor upon protonation. The protonation of the L_2X-type, η^5–Cp*, to form the L_2-type, diolefin η^4-Cp*H, leads to a change in coordination environment of the [Rh] center. Further addition of a H^+ source, such as protonated dimethylformamide ($[DMF{\cdot}H]^+[OTf]^-$), leads to hydrogen evolution and to the reformation of the starting complex. Additionally, Miller and co-workers have reported a similar [Rh] complex containing the η^4-Cp*H and bpy ligands (see Figure 1.3).[9]

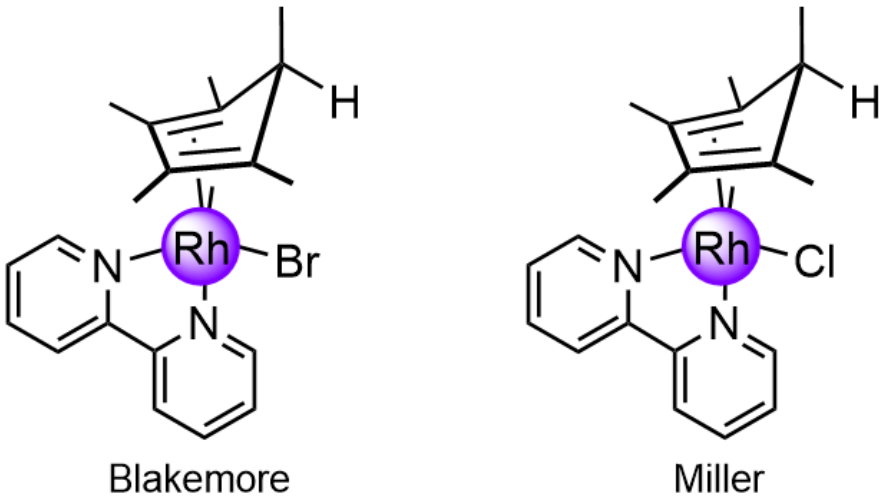

Figure 1.3: The proton-responsive Cp*H intermediates synthesized by Blakemore and Miller, intermediates in the pathway to hydrogen evolution.

Here, the Miller group initially wanted to explore the selective transfer of a hydride from the [Rh] complex to the enzyme cofactor nicotinamide adenine dinucleotide (NAD^+) to form 1,4-NADH, extending a bridge between transition metal catalysis and enzymatic

catalysis. However, they instead discovered additional evidence for Cp*H as an intermediate form of the compound that could be involved in NAD^+ reduction.

This class of catalysts are distinctive because they utilize both a redox active bpy ligand and a proton responsive Cp* ligand attached to the [Rh] center. Catalytic properties of the metal center are modulated upon protonation and deprotonation. Though [Rh] is an expensive metal, the work presented by Blakemore and Miller presents a rare opportunity to study in depth the fundamental reaction mechanism of coupling protons and electrons via this well-defined molecular catalyst. To improve upon the current catalyst design, certain changes need to be made to perturb the system, but not so drastically that we lose insight into the possible mechanism(s) of hydrogen evolution.

An attractive change would be the derivatization of the redox active bpy ligand. Specifically, changing the substituents at the 4,4′-position of the bpy ligand to make 4,4′-*tert*-butyl-2,2′-bipyridine (tBu-bpy) or 4,4′-trifluoromethyl-2,2′-bipyridine (CF_3-bpy), would provide more electron rich and electron poor ligands, respectively compared to the parent bpy ligand. By coordinating these different ligands to [Cp*Rh(L)Cl] we should be able to modulate the catalysts propensity toward H_2 evolution by making the Rh-center more basic (tBu-bpy) or acidic (CF_3-bpy). By making these substitutions to the bpy ligand, this will allow for a series of compounds to be studied, and for a structure-function relationship to be determined.

Here we report the synthesis and characterization of two novel [Rh] complexes based upon the parent proton-reduction catalyst [Cp*Rh(bpy)Cl] first described by Grätzel. These new compounds are then further evaluated using electrochemical techniques to

analyze their disposition toward hydrogen evolution catalysis, their Faradaic efficiency, and their turnover number.

Synthesis of Ligands and Complexes

All solvents were of commercial grade and dried over activated alumina using a Grubbs-type solvent purification system prior to use.[10] Rhodium chloride hydrate (Pressure Chemical Co.), 1,2,3,4,5-pentamethylcyclopentadiene (94%; Alfa Aesar), 2,2′-bipyrdiyl (99%; Oakwood) 4-*tert*-butyl-pyridine (96%; Aldrich), and 2-chloro-4-trifluoromethyl-pyridine (98%; Oakwood) were used as received. $[Cp^*RhCl_2]_2$, *tert*-butyl-bipyridine (tBu-bpy), and trifluoromethyl-bipyridine (CF_3-bpy) were prepared according to literature methods.[11,12,13] The commercial rhodium chloride hydrate and 1,2,3,4,5-pentamethlcyclopentadiene were used to synthesize $[Cp^*RhCl_2]_2$ (see Scheme 1.1).[11]

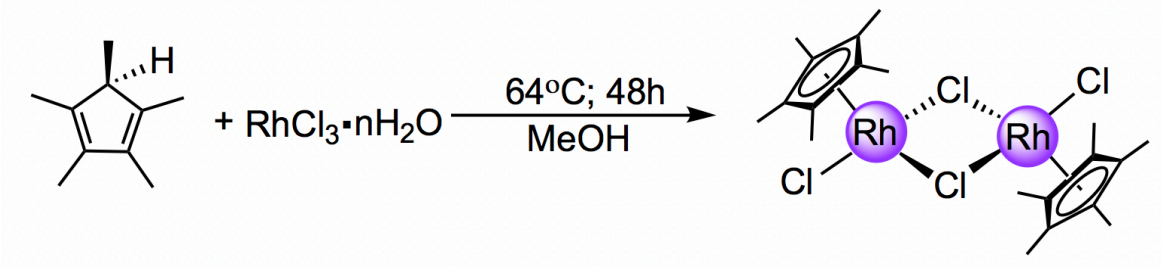

Scheme 1.1: Synthesis of $[Cp^*RhCl_2]_2$.

The commercial 4-*tert*-butylpyridine was used to synthesize 4-*tert*-butylpyridine-*N*-oxide, followed by the chlorination of this material to give 2-chloro-4-*tert*-butyl-pyridine. The chlorinated material was then used in an Ullmann-like coupling to afford the desired

tBu-bpy ligand.[12] Similarly, 2-chloro-4-trifluoromethyl-pyridine was used in an Ullmann-like coupling to prepare the CF_3-bpy ligand.[13] The tBu-bpy and CF_3-bpy ligands were purified via sublimation, 100°C at 1 mTorr and 70°C at 1 mTorr, respectively to obtain analytically pure material by ^{1}H NMR (see Scheme 1.2).

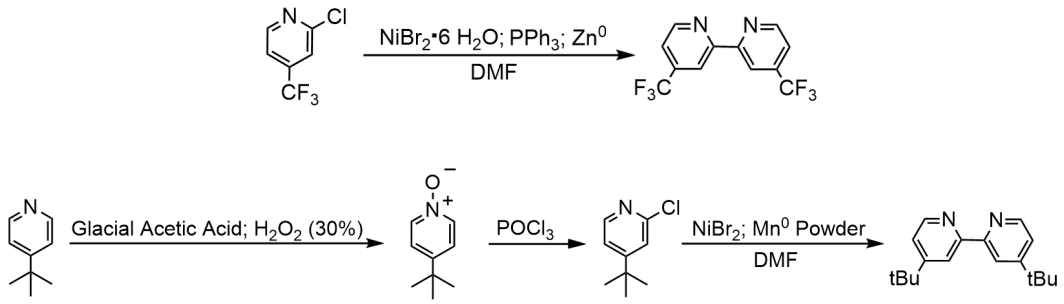

Scheme 1.2: Synthesis of the CF_3-bpy and tBu-bpy ligands.

These compounds were then dried and brought into an inert atmosphere glovebox before synthesizing complexes **1**, **2**, and **3 (**See Scheme 1.3, below).

Complexes **1**, **2**, and **3** were prepared according to literature procedures of similar complexes, and in an inert atmosphere glovebox.[3] To a 20 mL scintillation vial equipped with a Teflon stir bar, $[Cp^*RhCl_2]_2$ (1 equiv.) was dissolved in MeCN (ca. 4mL) to give a deep red solution. To this solution, $AgPF_6$ (2 equiv.) in MeCN (ca. 2mL) was added, resulting in an orange solution with AgCl as a white precipitate. The solution was allowed to stir for 10 min. Then the appropriate bipyridine-based ligand (2 equiv.) was dissolved in, MeCN (ca. 2mL) for **2** and **3** and THF (ca. 2 mL) for **1**, and was added to the orange solution. Upon addition, the solution lightens to a yellow-orange color and is allowed to stir for 15 min. The AgCl precipitate was then filtered off and the resulting yellow solution in the filter flask was placed in a scintillation vial. Diethyl ether was then

added to the solution in the scintillation vial to precipitate the desired product. The yellow solid was then filtered through fritted glass to afford, **1**, **2**, and **3**, in 94%, 60%, and 59% yield, respectively. Complexes **1** and **3** were fully characterized using ^{1}H NMR, ^{13}C NMR, ^{31}P NMR, ESI mass spectrometry, UV-vis, and single crystal X-ray diffraction (XRD).

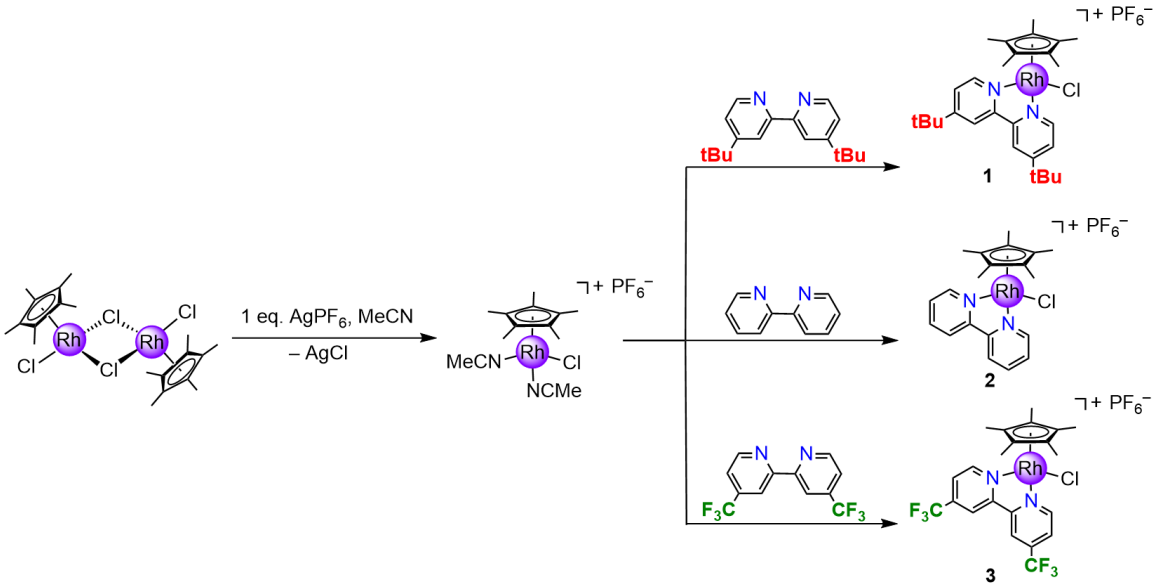

Scheme 1.3: Synthetic scheme of the synthesized [Rh] complexes bearing the substituted bpy ligands.

NMR Spectroscopic Studies

Nuclear magnetic resonance (NMR) spectroscopic studies of **1** confirmed the structure and purity of the sample. The ^{1}H-NMR spectrum shows two singlets in the aliphatic region. The singlet at 1.45 ppm corresponds to the two tBu-groups (s, 18H). The singlet at 1.66 ppm corresponds to the freely-rotating Cp*-ring, making the methyl groups equivalent (s, 15H). The peaks in the aromatic region correspond to the bipyridine moiety. A doublet is observed at 8.75 ppm (d, $^{3}J_{H\text{-}H}$ = 6.0 Hz, 2H) corresponding to H-

atom type 1 (see Figure). The doublet at 8.36 ppm ($d_{H\text{-}H}$, $^{3}J_{H\text{-}H}$ = 2.0 Hz, 2H) corresponds to H-atom type 2. The doublet of doublets at 7.78 ppm (dd, $^{3}J_{H\text{-}H}$ = 6.0Hz, $^{4}J_{H\text{-}H}$ = 2.1 Hz, 2H) corresponds to H-atom type 3. This molecule behaves with C_{2v} symmetry in solution and thus has a mirror plane bisecting the bipyridine, giving rise to only three distinct peaks for the six protons in the aromatic ring and one peak for the fifteen protons of the Cp* ring (see Figure 1.4).

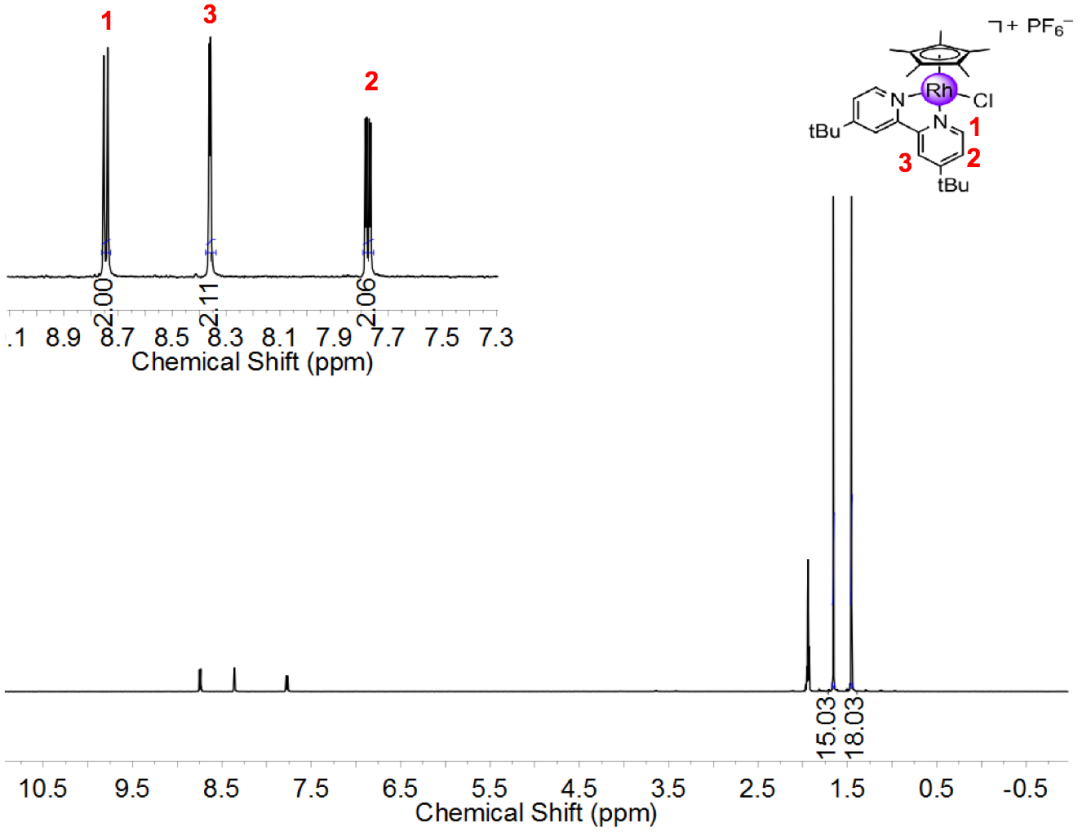

Figure 1.4: ^{1}H-NMR (400 MHz, CD_3CN) spectrum of $[Cp^*Rh(tBu\text{-}bpy)Cl]^{+}(PF_6)^{-}$.

Additionally, we can confirm that the tBu-bpy ligand has coordinated to the [Rh] metal center due to an observed change in chemical shift between free-ligand and the complex (see Figure 1.5).

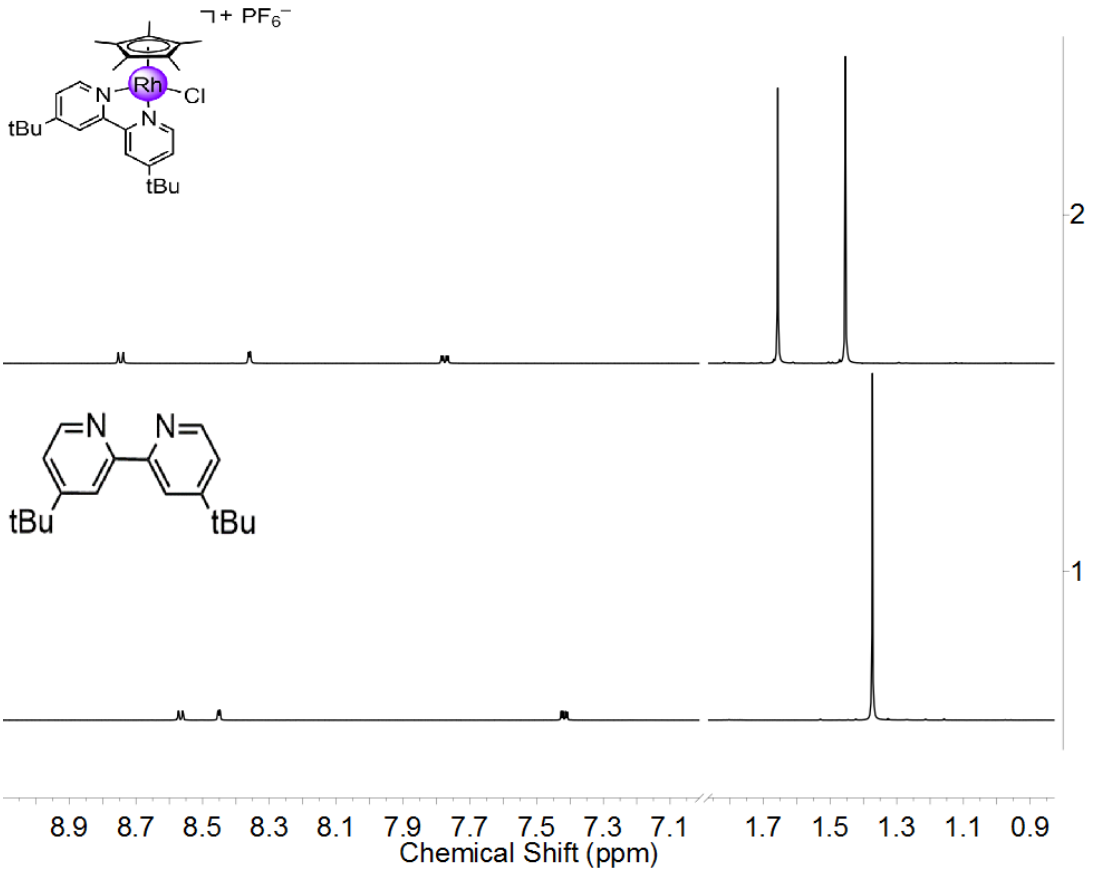

Figure 1.5: ^{1}H-NMR (400 MHz, CD_3CN) spectrum of $[Cp^*Rh(tBu\text{-}bpy)Cl]^{+}(PF_6)^{-}$ and the free ligand, tBu-bpy.

The chemical shift for the peaks of the tBu-ligand, once coordinated to the metal center, move downfield in the spectrum. Notably, not only did the aromatic peaks shift but the singlet corresponding to the *tert*-butyl groups on the ligand has also shifted. This is because the Lewis acidic Rh^{III} center is electron deficient and upon binding the ligand donates electron density to the metal center, contributing to a deshielding effect, consistent with what is observed in the ^{1}H-NMR spectrum.

The ^{13}C-NMR spectrum shows nine distinct peaks as expected, with two peaks from the Cp* ring, five peaks from the bipyridine-moiety, and two peaks from the *tert*-butyl groups. Since [Rh] has a nuclear spin of $\frac{1}{2}$ there is an observable doublet at 97.5 ppm (d, $^{3}J_{\text{C-Rh}}$ = 8.0 Hz) due to C-Rh coupling (see Figure 1.6).

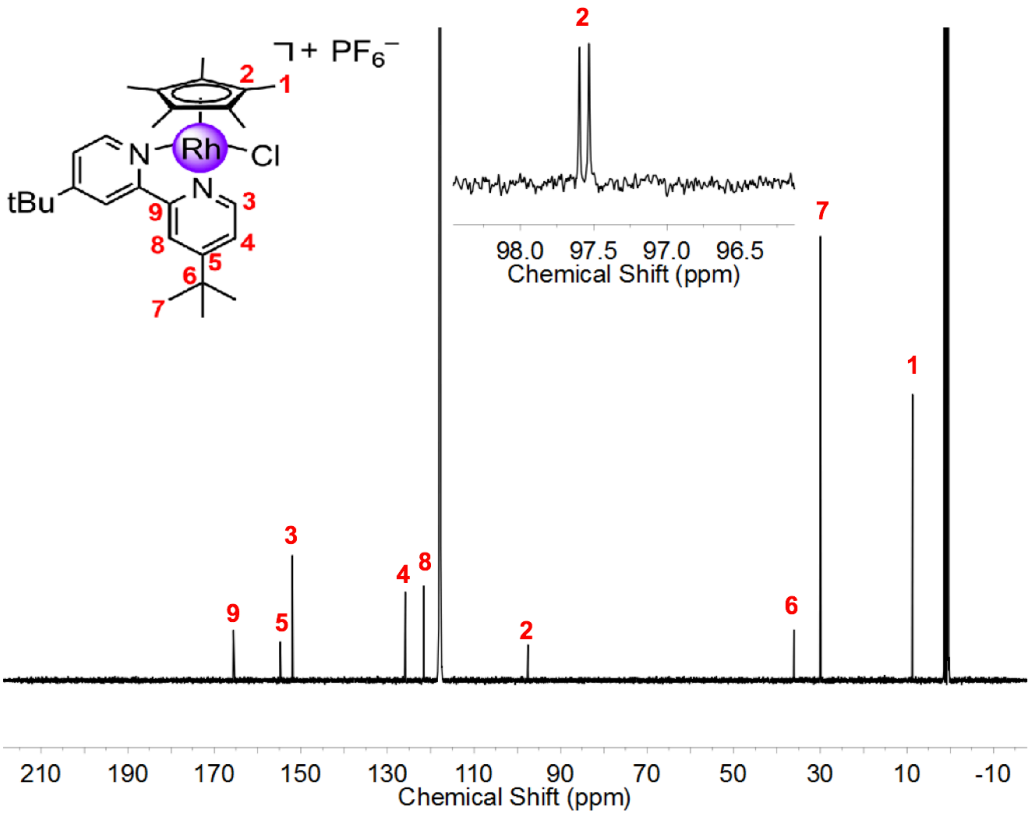

Figure 1.6: ^{13}C{^{1}H}-NMR (126 MHz, CD_3CN) spectrum of $[Cp^*Rh(tBu\text{-}bpy)Cl]^{+}(PF_6)^{-}$.

The ^{31}P-NMR spectrum exhibits a distinct septet at -144.6 ppm (m, $^{1}J_{\text{P-F}}$ = 699.7 Hz) arising from the PF_6^- counteranion. The septet occurs due to fluorine, which has a nuclear spin of $\frac{1}{2}$, coupling with phosphorus. Since there are six fluorine atoms attached to phosphorus this is observed as a septet in the spectrum (see Figure 1.7).

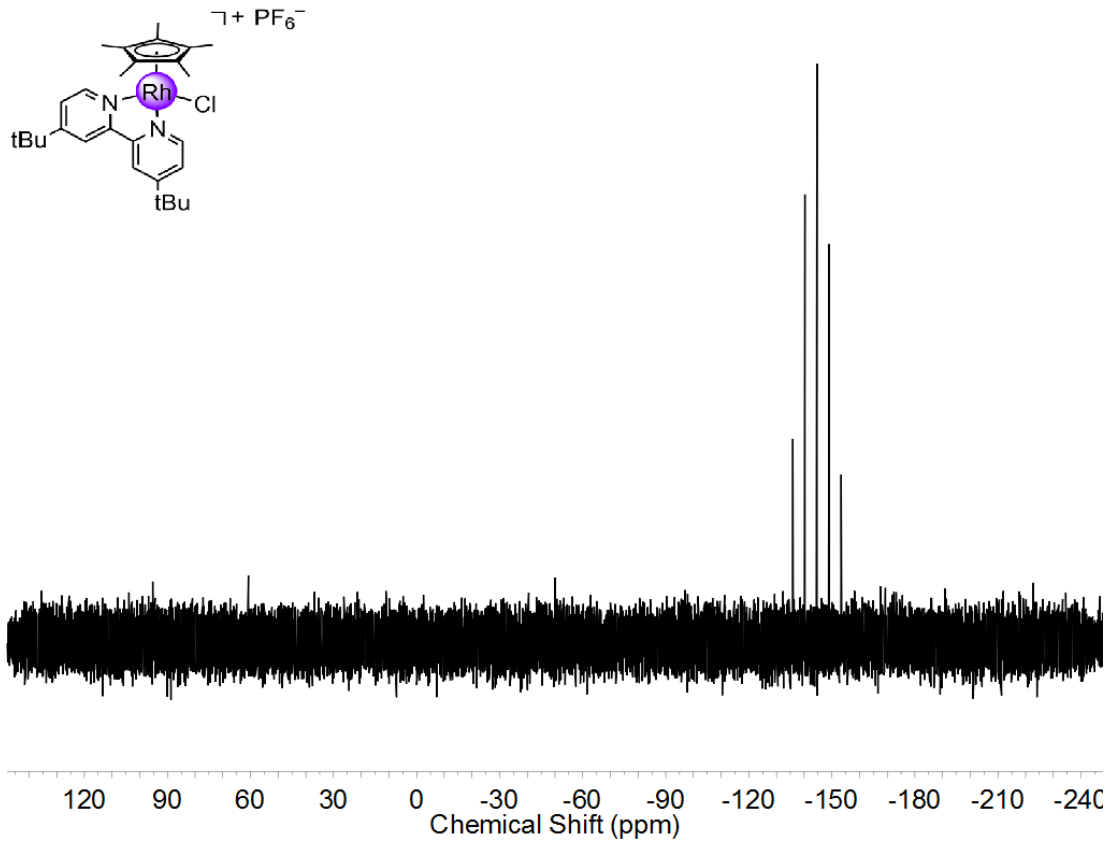

Figure 1.7: $^{31}P\{^{1}H\}$-NMR (162 MHz, CD_3CN) spectrum of $[Cp^*Rh(tBu\text{-}bpy)Cl]^+(PF_6)$.

The observed signals for the ^{1}H, ^{13}C, and ^{31}P- NMR spectra confirm the structure, purity, and existence of **1**.

NMR spectroscopic studies of **3** also confirmed the structure and purity of the sample. Like molecule **1**, this molecule also has C_{2v} symmetry in solution and thus has a mirror plane bisecting the bipyridine, giving rise to only three distinct peaks for the six protons in the aromatic ring and one peak for the fifteen protons of the Cp* ring (see Figure 1.8). The ^{1}H-NMR shows one singlet in the aliphatic region at 1.69 ppm, which corresponds to the freely-rotating Cp*-ring, resulting in the methyl groups being equivalent (s, 15H). The peaks in the aromatic region correspond to the bipyridine moiety. A doublet is observed at 9.11 ppm (d, $^{3}J_{H\text{-}H}$ = 5.8 Hz, 2H) corresponding to H-atom type 1 (see below). The

doublet at 8.83 ppm (d, $^{3}J_{H\text{-}H}$ = 1.8 Hz, 2H) corresponds to H-atom type 2. The doublet of doublets at 8.14 ppm (dd, $^{3}J_{H\text{-}H}$ = 5.8 Hz, $^{4}J_{H\text{-}H}$ = 1.8 Hz, 2H) corresponds to H-atom type 3.

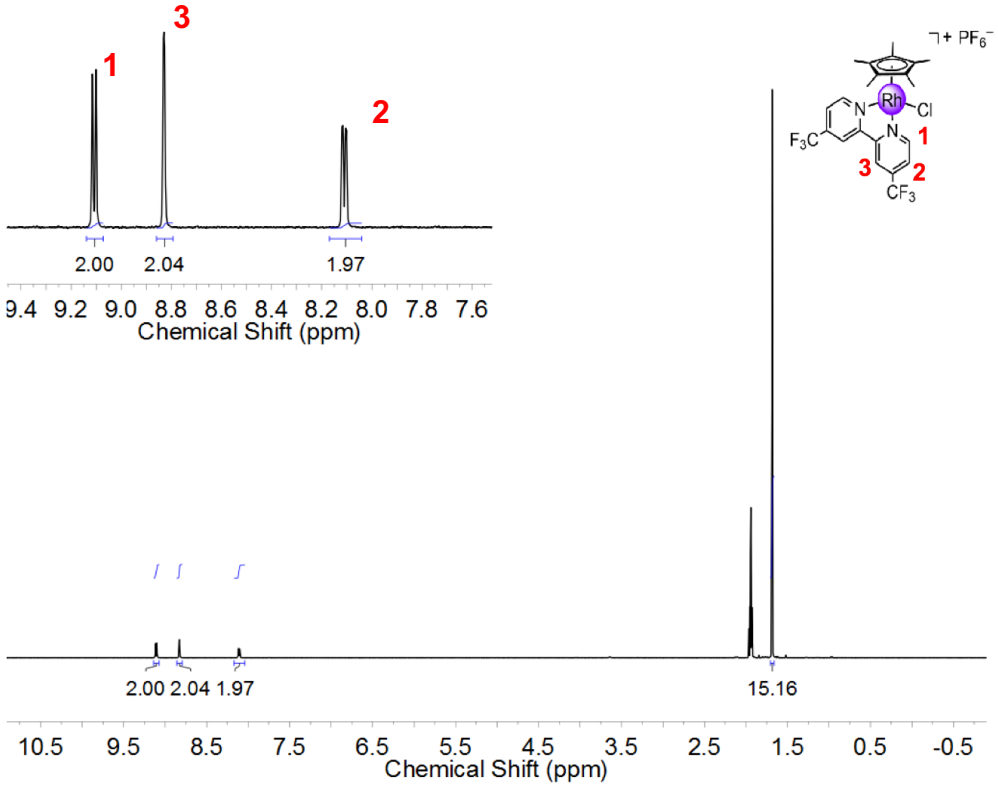

Figure 1.8: ^{1}H-NMR (400 MHz, CD_3CN) spectrum of $[Cp^*Rh(CF_3\text{-bpy})Cl]^{+}(PF_6)^{-}$.

Additionally, we can confirm that the CF_3-bpy ligand has coordinated to the Rh metal center due to an observed change in chemical shift between the free ligand and the complex (see Figure 1.9).

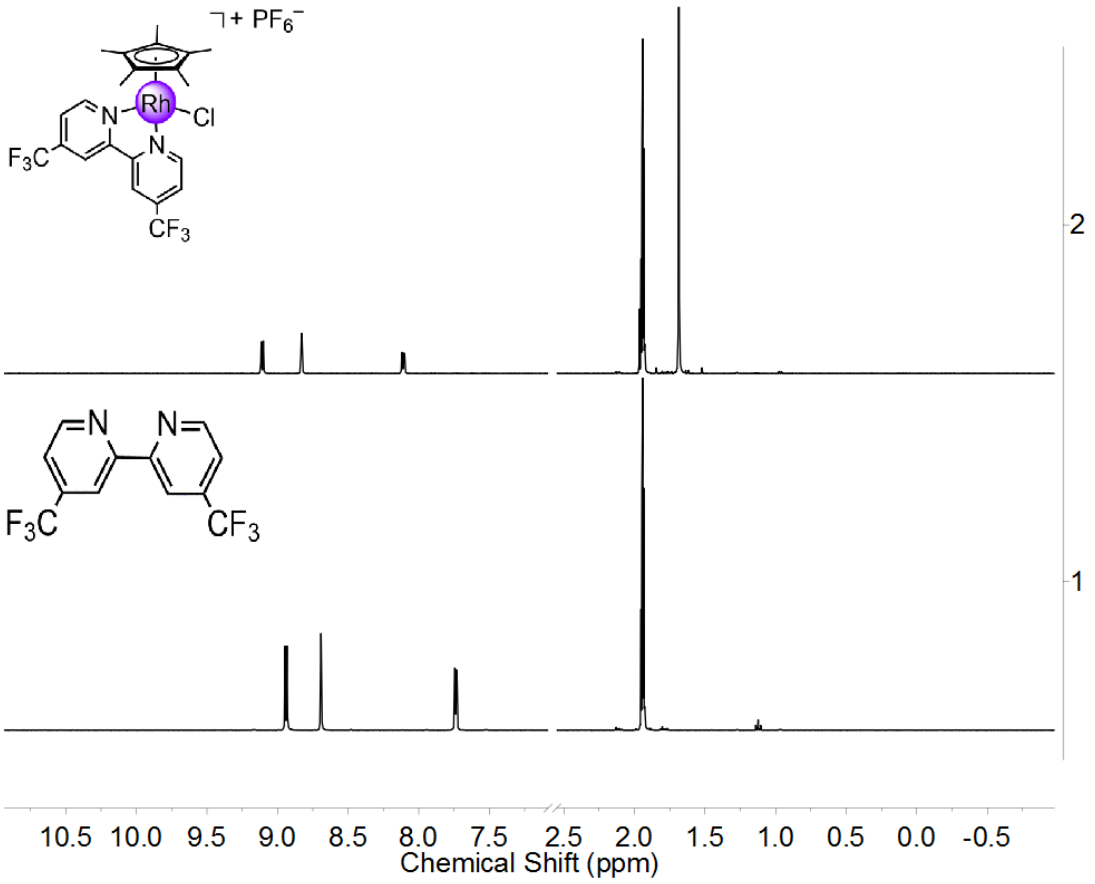

Figure 1.9: ^{1}H-NMR (400 MHz, CD_3CN) spectrum of $[Cp^*Rh(CF_3\text{-bpy})Cl]^{+}(PF_6)^{-}$ and the free ligand, CF_3-bpy.

The chemical shift for the peaks of the CF_3-ligand, once coordinated to the metal center, move downfield in the spectrum. As in the case for **1**, this is also because the Lewis acidic Rh^{III} center is electron deficient and upon binding the ligand donates electron density to the metal center, contributing to a deshielding effect, consistent with what is observed in the ^{1}H-NMR spectrum.

The ^{13}C-NMR shows eight distinct peaks as expected, with two peaks from the Cp*-ring, five peaks from the bipyridine-moiety, and one peak from the trifluoromethyl groups. Since [Rh] has a spin of $\frac{1}{2}$ there is an observable doublet at 98.8 ppm (d, $^{3}J_{\text{Rh-C}}$ = 8.2 Hz) due to C-Rh coupling. Since fluorine has a spin of $\frac{1}{2}$, there is observable carbon-

fluorine coupling. As a result there are also three individual quartets at 121.6 ppm (q, $^{3}J_{C\text{-}F}$ = 3.5 Hz) 125.3 ppm (q, $^{3}J_{C\text{-}F}$ = 3.4 Hz) and 141.5 ppm (q, $^{1}J_{C\text{-}F}$ = 35.9 Hz) (see Figure 1.10).

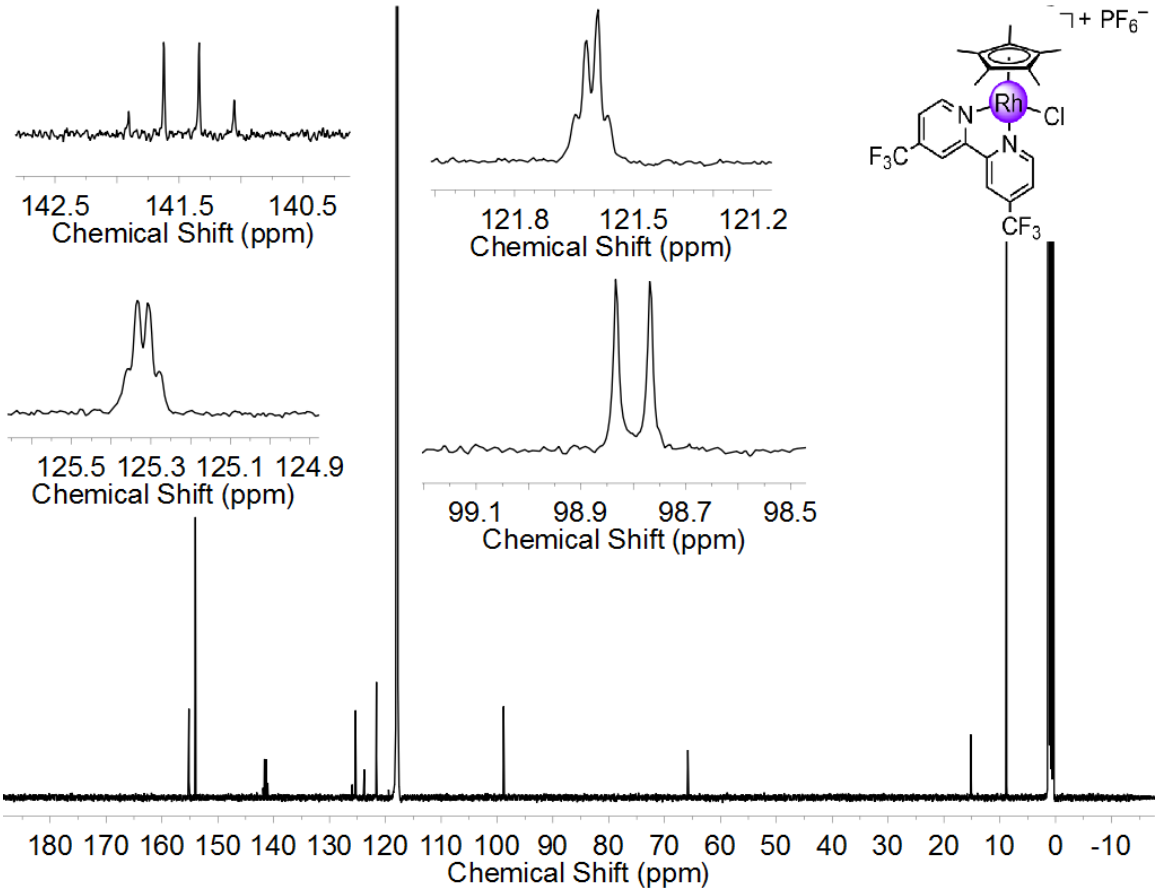

Figure 1.10: $^{13}C\{^{1}H\}$-NMR (126 MHz, CD_3CN) spectrum of $[Cp^*Rh(CF_3\text{-}bpy)Cl]^{+}(PF_6)^{-}$.

The peak splitting here makes the assignment for the ^{13}C-NMR more difficult and ambiguous. In order to make a clear assignment for each of the carbons on $[Cp^*Rh(CF_3\text{-}bpy)Cl]^{+}PF_6^{-}$ a 2D-NMR experiment was conducted.

Heteronuclear single quantum coherence (HSQC) spectroscopy is a 2D NMR technique that can be used to analyze molecules with multiple nuclei that exhibit complicated spectral splitting patterns.[14] The HSQC performed here was $^{1}H\text{-}^{13}C$ HSQC,

which provides correlation between carbon nuclei and its corresponding attached proton. The x-axis consists of a ^{1}H-NMR with units of chemical shift and the y-axis has a ^{13}C-NMR with units of chemical shift. The resulting spectrum displays signals where coupling between ^{13}C and ^{1}H nuclei occurs; these signals show the connectivity of the protons and carbons. Furthermore, the phasing of the cross-peaks indicates whether the peaks correspond to a methyl (–CH_3) or methine (–CH) group (positive, red in Figure 1.11) or to a methylene (–CH_2; negative, blue). This technique was used to elucidate the assignment of the ^{1}H-NMR and ^{13}C-NMR resonances for the $[Cp^{*}Rh(CF_3\text{-bpy})Cl]^{+}(PF_6)^{-}$ complex due to the intricate splitting of the ^{13}C-NMR spectrum. Since the proton NMR has distinct splitting in the aromatic region, the resulting points of intersection are used to correctly assign the ^{13}C-NMR spectrum (see Figures 1.11-1.12).

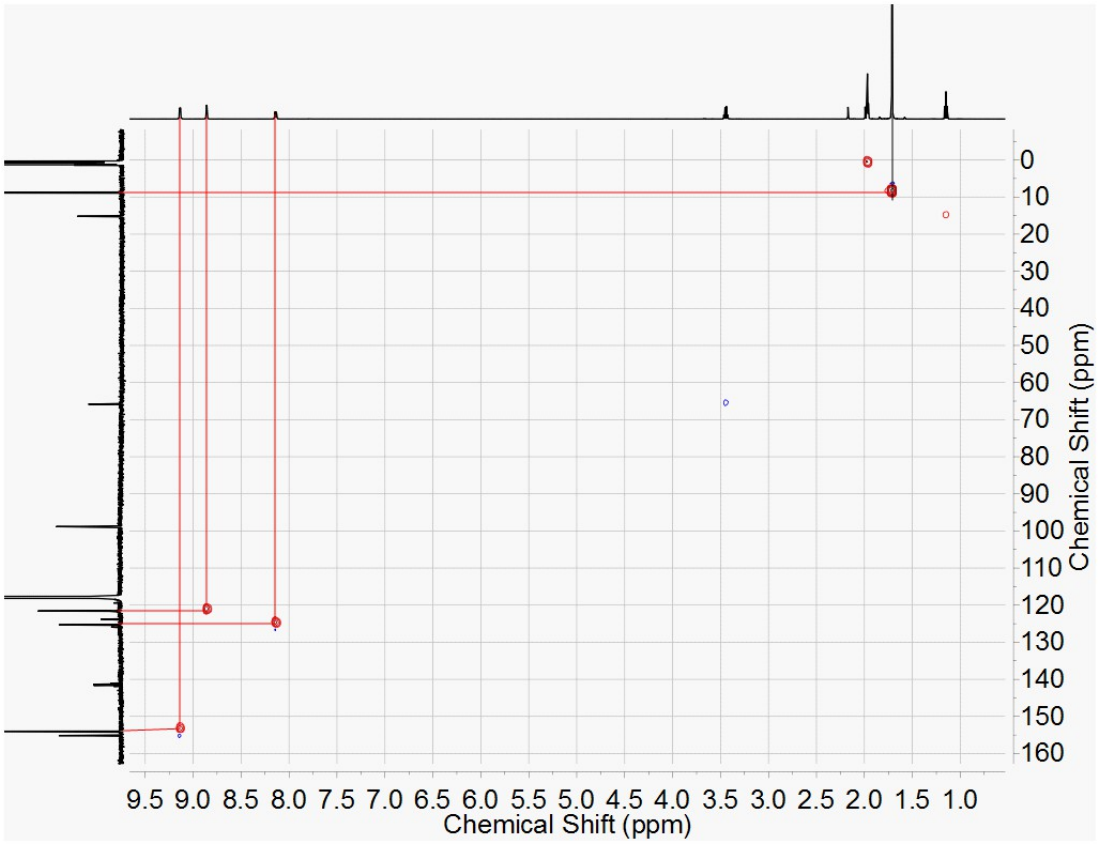

Figure 1.11: ^{1}H-^{13}C HSQC for $[Cp^{*}Rh(CF_3\text{-bpy})Cl]^{+}(PF_6)^{-}$ with solvent CD_3CN.

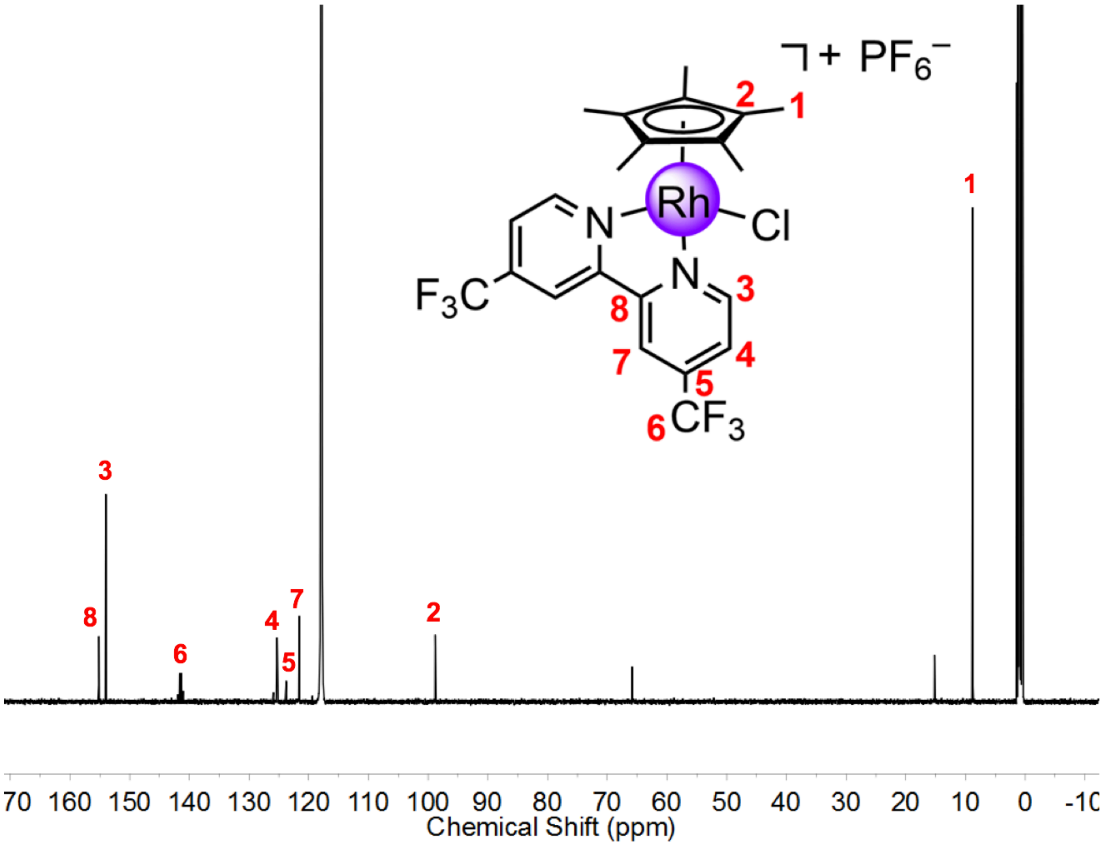

Figure 1.12: Assignment of the $^{13}C\{^{1}H\}$-NMR (126MHz, CD_3CN) spectrum of $[Cp^*Rh(CF_3\text{-bpy})Cl]^+(PF_6)^-$.

The ^{19}F-NMR shows two distinct peaks as expected, with one peak from the CF_3-bpy moiety of the [Rh] complex, and one from the PF_6^- counteranion. The symmetry and free rotation of the trifluoromethyl fluorines on **3** result in the singlet at -65.4 ppm (s). The PF_6^- counteranion has six equivalent fluorines attached to phosphorus, which has a nuclear spin of $\frac{1}{2}$, resulting in a doublet at -72.9 ppm (d, $^1J_{F\text{-}P}$ = 706.6 Hz) (see Figure 1.13)

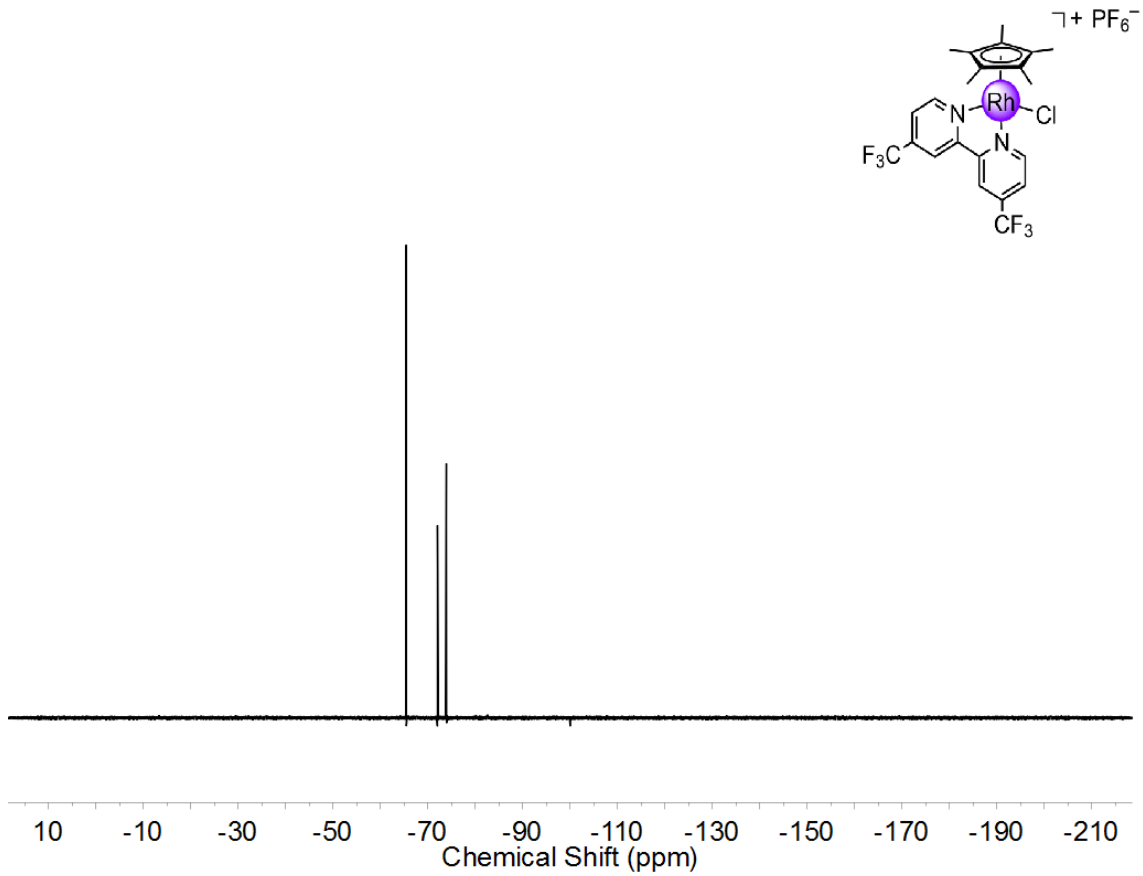

Figure 1.13: ^{19}F-NMR (376MHz, CD_3CN) spectrum of $[Cp^*Rh(CF_3\text{-bpy})Cl]^+(PF_6)^-$.

The ^{31}P-NMR shows one distinct septet as expected. This is due to the PF_6^- counteranion and because six fluorines are bound to the phosphorus, each having a nuclear spin of $\frac{1}{2}$, this results in the observable septet at -144.7 ppm (m, $^1J_{P\text{-}F}$ = 700.2 Hz) (see Figure 1.14).

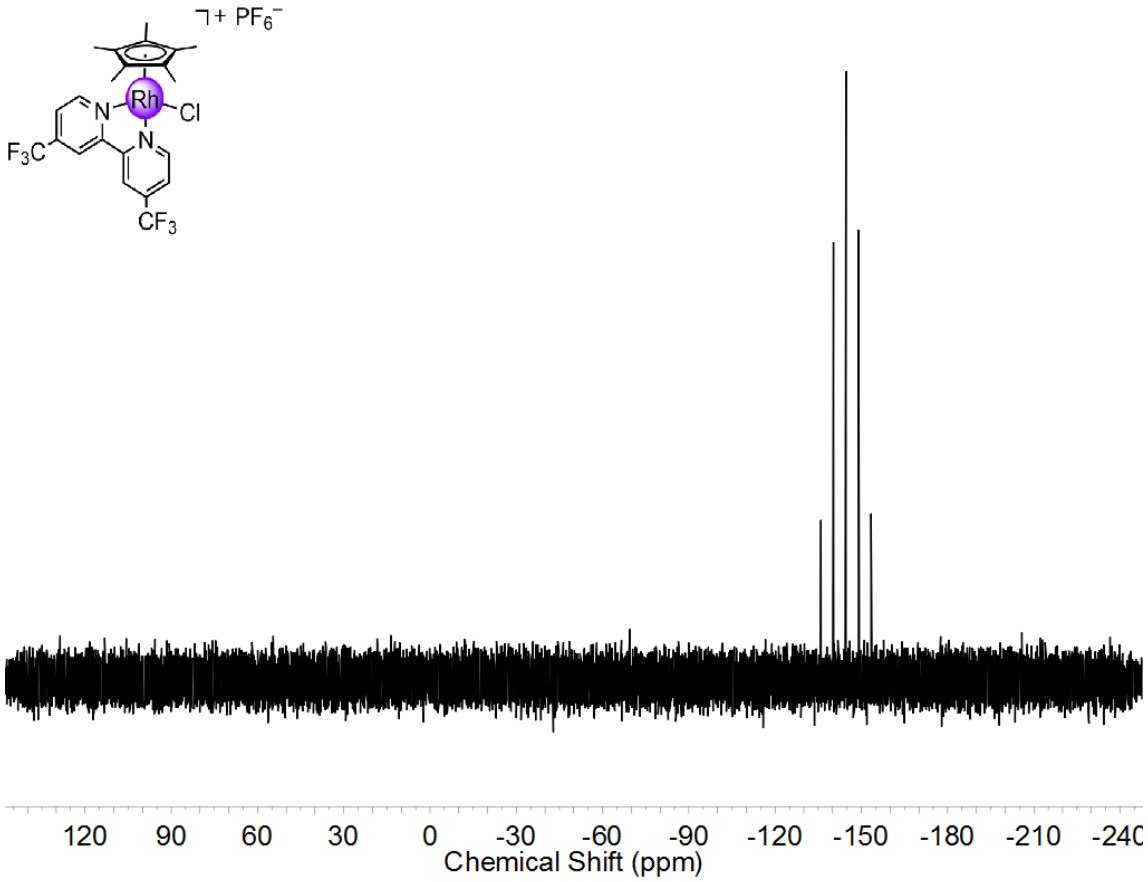

Figure 1.14: $^{31}P\{^{1}H\}$-NMR (162MHz, CD_3CN) spectrum of $[Cp^*Rh(tBu\text{-}bpy)Cl]^+(PF_6)^-$.

The observed signals for the ^{1}H, ^{13}C, ^{19}F, ^{31}P, and HSQC-NMR spectra confirm the structure, purity, and existence of compound **3**.

Mass Spectrometry Studies

The mass spectrum of **1** revealed four prominent fragments, including the molecular ion (M^+) peak at 541.18 m/z. The experimental mass spectrum shows excellent agreement with the predicted mass spectrum. The mass spectrum of **3** also revealed four prominent fragments, including the M^+ peak at 565.03 m/z. The experimental spectrum also shows exceptional agreement with the predicted spectrum. Since ^{13}C has a 1.1%

natural abundance, a fragment corresponding to the molecular ion peak plus 1 m/z is observed. Notice, both complexes contain a chloride attached to [Rh] resulting in an observable fragmentation pattern for ^{35}Cl and ^{37}Cl isotopes, which are naturally present at 75% and 25% abundance, respectively (see Figures 1.15-1.16).[15]

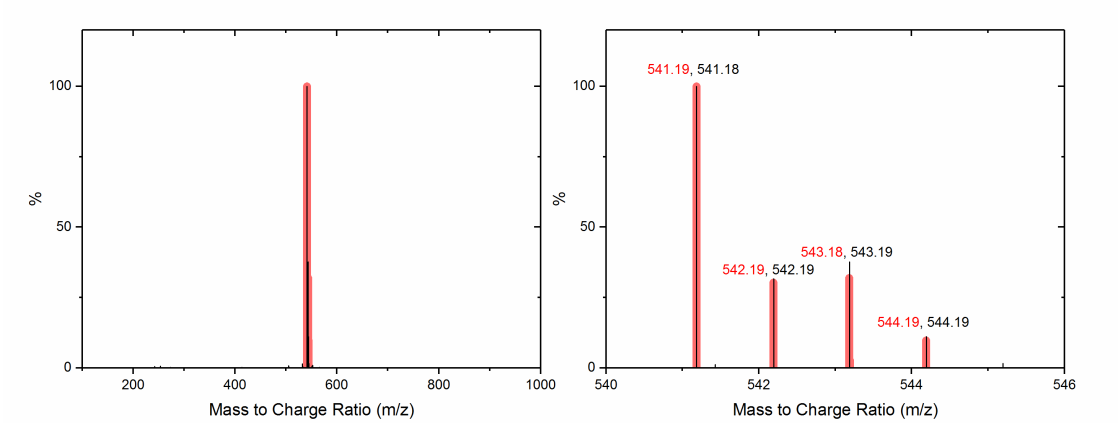

Figure 1.15: The predicted and experimental mass spectrum fragmentation of $[Cp^*Rh(tBu\text{-}bpy)Cl]^+(PF_6)^-$ (**1**), predicted (red) and experimental (black).

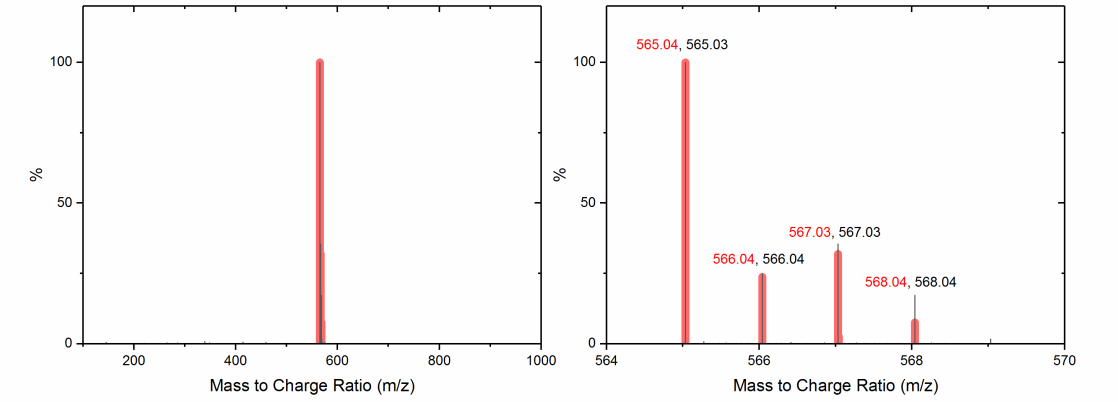

Figure 1.16: The predicted and experimental mass spectrum fragmentation of $[Cp^*Rh(CF_3\text{-}bpy)Cl]^+(PF_6)^-$ (**3**), predicted (red) and experimental (black).

Electronic Absorption Spectroscopic Studies

The UV-vis spectrum of **1** in MeCN reveals four distinct peaks in the UV-region and one peak that has a shoulder that trails off into the visible region. This shoulder in the

visible region is responsible for this compound's bright-yellow color (λ = 348.1nm, ε = 3800 mol L^{-1} cm^{-1}). The UV-visible spectrum of **3** also shows four distinct peaks in the UV-region and one peak that has a shoulder that tracts into the visible region. This shoulder in the visible region is responsible for the bright-yellow color observed (λ = 374.7 nm, ε = 2900 mol L^{-1} cm^{-1}) (see Figure 1.17).

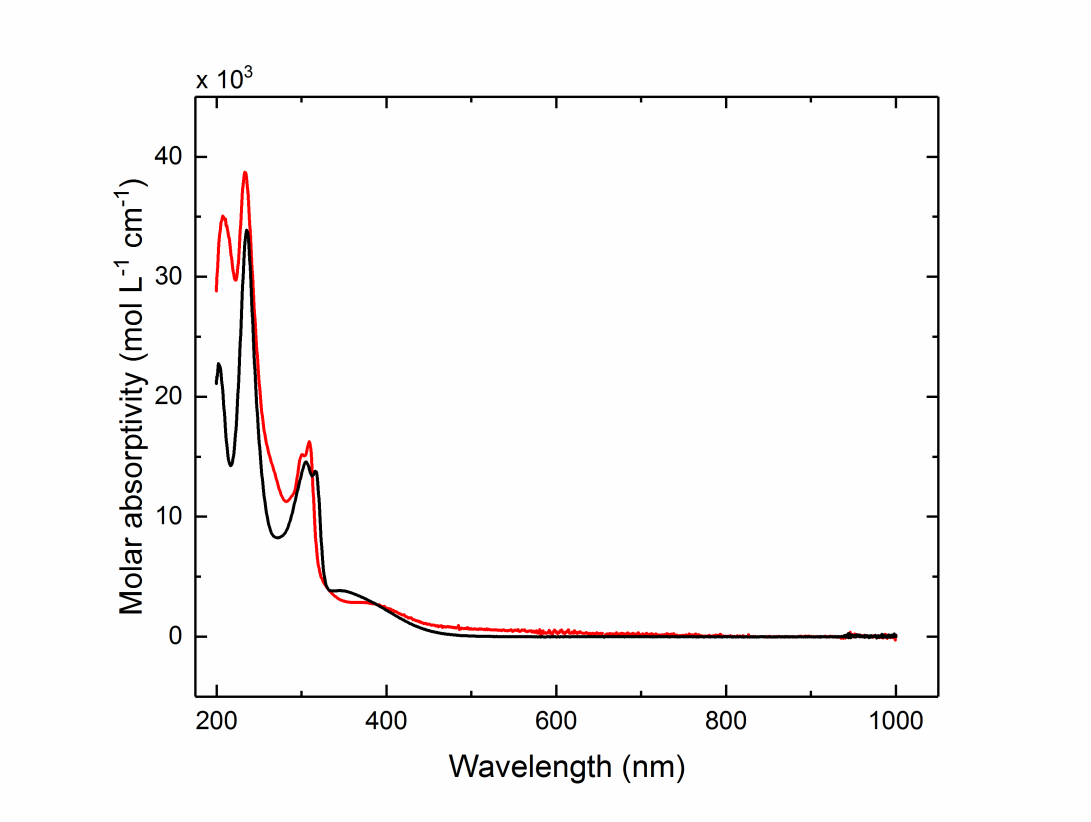

Figure 1.17: UV-visible spectrum of **1** (red line) and **2** (black line).

X-ray Crystallography

Crystals of **1** and **3**, suitable for X-ray diffraction, were obtained by vapor diffusion of diethyl ether into acetonitrile. Crystals of **1** were red plates of rectangular morphology contained within a tetrahedral crystal system. The [Rh] center is coordinated by tBu-bpy,

Cp*, and chloride ligands in a tetrahedral-like geometry (see Figure 1.18). The complex crystallized in the I4/m space group. In the solid state, the complex possesses C_s symmetry, which is consistent with its solution behavior as observed by NMR spectroscopy. The Rh–N1 and Rh–N2 bond distances are identical, 2.102(5) Å, due to a crystallographic mirror plane bisecting the Cp* ring, the chloride, and the tBu-bipyridine ligand. The distance between [Rh] and the centroid of Cp* is 1.79 Å. The observed Rh-Cl distance is 2.380(2) Å, which is comparable to a similar [Cp*RhCl] bipyridine-based complex reported by Scharwitz and co-workers.[16] An outer-sphere hexafluorophosphate counteranion was also observed, which balances the +1 charge of **1**.

Crystals of **3** were also red plates. However, this structure has not yet been refined, so only preliminary bond lengths will be reported (see Figure 1.18). The point group of this molecule is *pseudo*-C_s, in the solid state because a crystallographic plane of symmetry does not bisect the CF_3-bpy ligand. The Rh-N1 and Rh-N2 are 2.091 Å and 2.135 Å, respectively. The distance between [Rh] and the centroid of the Cp* ring is also 1.79 Å. The observed Rh-Cl distance is 2.371 Å. The preliminary crystal structure also shows an outer-sphere hexafluorophosphate counteranion to balance the +1 charge of **3**. Comparisons can be better made between the two complexes, and previously made complexes, once the structure is fully refined.

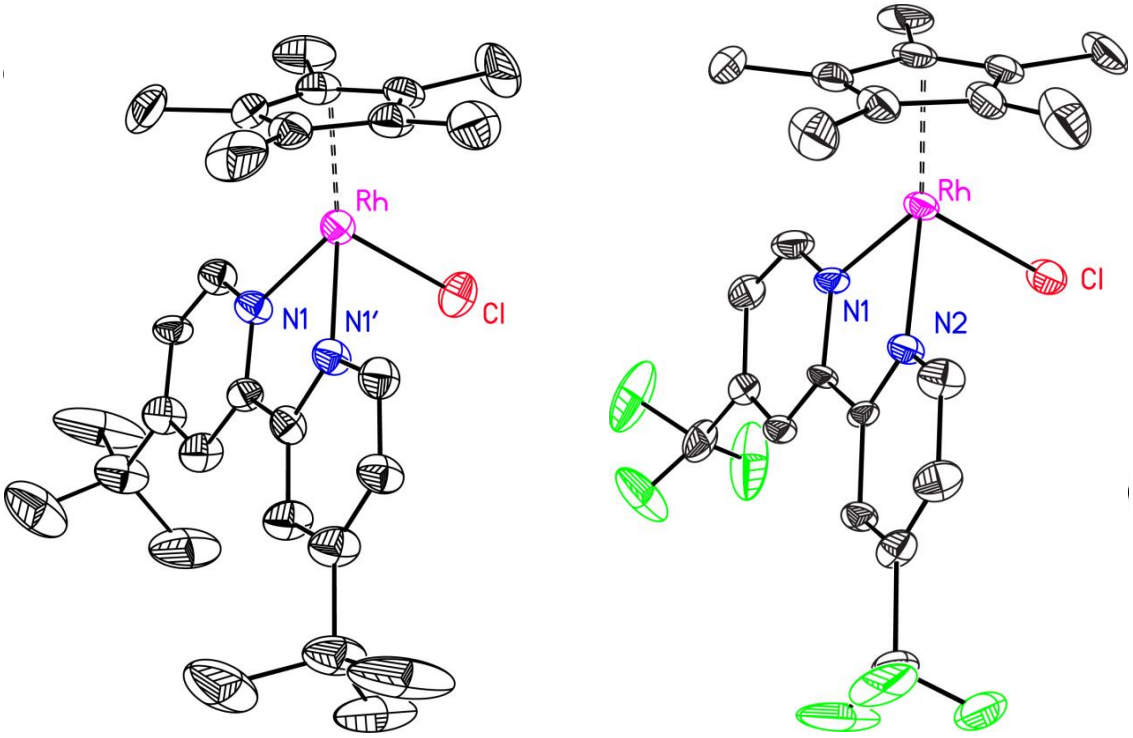

Figure 1.18: Crystal structures of **(1)**, $[Cp^*Rh(tbu\text{-}bpy)Cl]^+ (PF_6)^-$ (left) and **(3)**, $[Cp^*Rh(CF_3\text{-}bpy)Cl]^+ (PF_6)^-$ (right) obtained from X-ray diffraction. Displacement ellipsoids shown at 50% probability.

Electrochemical Studies: Cyclic Voltammetry

Cyclic voltammograms (CVs) of **1** and **3** were performed in an inert atmosphere glovebox using a Gamry Reference 600+ potentiostat. A three-electrode system was utilized, which consisted of a basal plane graphite (BPG) working electrode, platinum wire counter electrode, and silver quasi-reference electrode. The electrolyte used was 0.1 M electrochemistry-grade $n Bu_4N^+PF_6^-$ in MeCN. Previously, Grätzel et al. reported the electrochemistry of **2**.[3] They observed a single, reversible reduction event, which was assigned as a $2e^-$ reduction of the six coordinate, $18e^-$, $[Cp^*Rh^{III}(bpy)Cl]^+PF_6^-$, resulting in a five-coordinate, $18e^-$, $Cp^*Rh^I(bpy)$ complex. The five-coordinate $18e^-$ complex was

also prepared chemically, and has since been confirmed as an intermediate in the catalytic cycle for hydrogen evolution.[8]

We were able to successfully reproduce the electrochemical results of Grätzel et al. for complex **2,** which demonstrated the known $2e^-$ redox couple, $E_{1/2}$ = –1.21 V vs. $Fc^{+/0}$, which is assigned as a reversible $Rh^{III/I}$ couple.[3] For the newly synthesized [Rh] complexes, a $2e^-$ virtually reversible reduction event is observed for **1** at $E_{1/2}$ = –1.25 V vs. $Fc^{+/0}$. Based on the charge passed in voltammetry in comparison to a solution of ferrocene of known concentration, we estimate two electrons transferred per rhodium complex in the observed reduction wave. In analogy to the known behavior of **2**, we assign the observed reduction of **1** to a $Rh^{III/I}$ couple. This $E_{1/2}$ is more negative than that observed for the parent complex **2**, as expected due to the presence of the electron-donating *tert*-butyl substituents on the bpy ligand. By introducing these *tert*-butyl groups we have effectively made the [Rh] center more electron-rich and as a result, more difficult to reduce. A $2e^-$ redox couple is also observed for **3**, $E_{1/2}$ = –0.97 V vs. $Fc^{+/0}$, which is also assigned to a reversible $Rh^{III/I}$ couple. This $E_{1/2}$ is more positive than that observed for the parent complex, **2**, which is expected, due to the electron-withdrawing trifluoromethyl substituents on the bipyridine ligand. By introducing these functional groups we have modified the [Rh] center to be more electron-poor and concurrently, more easy to reduce, compared to the parent complex, **2**. The electrochemical behavior of the new complexes resembles the previously reported parent complex. The reduction event appears to be more reversible for the electron donating ligands, which is expected because the metal center is more electron rich and is thus easier to oxidize. The converse is true for electron withdrawing ligands, where the metal center is more electron deficient

and consequently more difficult to oxidize. This is apparent when we compare the peak to peak separation (ΔE_p), showing that **1** is the most reversible (see Figure 1.19).

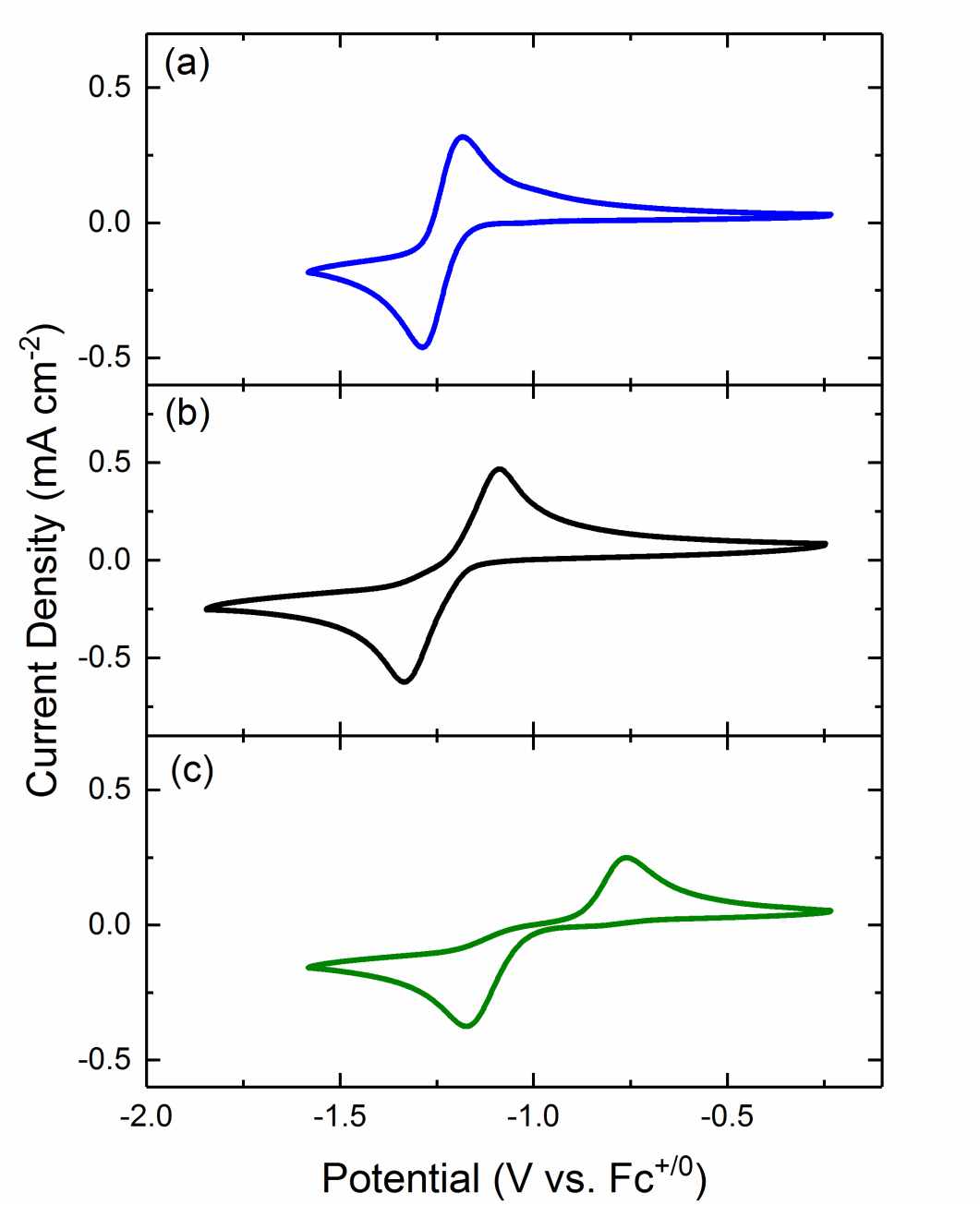

Figure 1.19: CVs of complexes **(a)** $[Cp^*Rh(tBu\text{-}bpy)Cl]^+PF_6^-$ (ΔE_p = 105.8 mV , **(b)** $[Cp^*Rh(bpy)Cl]^+PF_6^-$ (ΔE_p = 244.9 mV, and **(c)** $[Cp^*Rh(CF_3bpy)Cl]^+PF_6^-$ (ΔE_p = 413.8 mV), directly comparing there standard reduction potentials vs. $Fc^{+/0}$.

Since both processes are reversible we can easily carry out a scan rate dependence study to determine if the new complexes are freely diffusing in solution in both their oxidized and reduced forms. This is important because we are showing that the complex does not become permanently attached to the working electrode surface, but is rather actively diffusing to and from the surface of the electrode. The complex is termed diffusional if the peak currents of the anodic and cathodic waves of the CV are linear, compared to the square root of the scan rate; this relationship is based on the Randles-Sevčik equation.[17] In the equation below, i_p is the peak current, n is the number of electrons transferred in the redox event, F is Faraday's constant, A is the area of the electrode, C is the concentration of analyte, D is the diffusion coefficient, v is the scan rate, R is the ideal gas constant, and T is the temperature (see equation 1.4). Both the new complexes were determined to be diffusional in this way (see Figures 1.20-1.21).

$$i_p = Constant\ nFAC(\sqrt{\frac{nFvD}{RT}}) \quad (1.4)$$

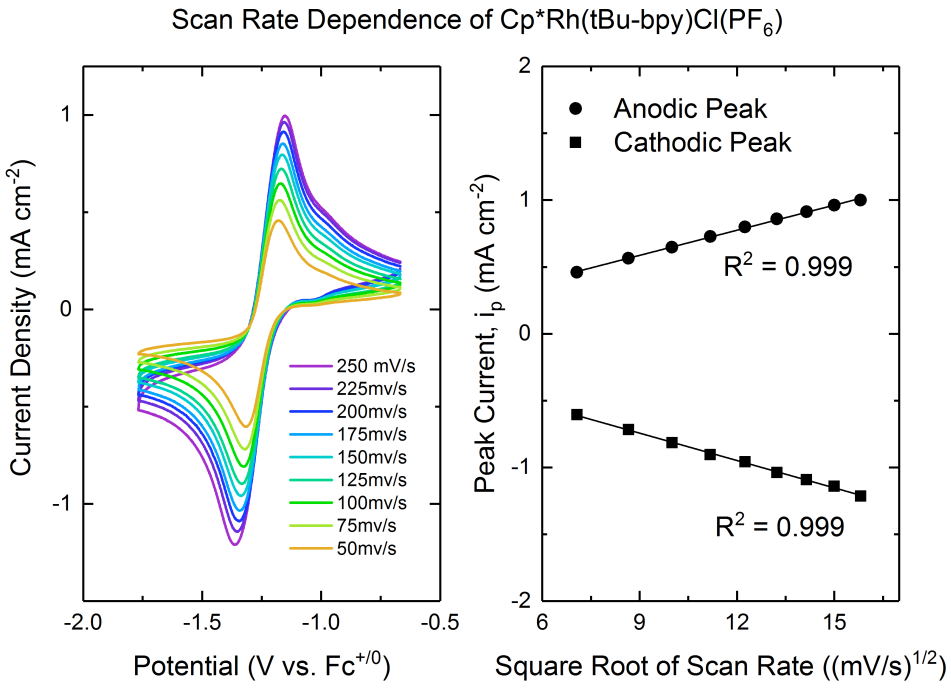

Figure 1.20: Scan rate dependence of **1,** illustrating a diffusional process.

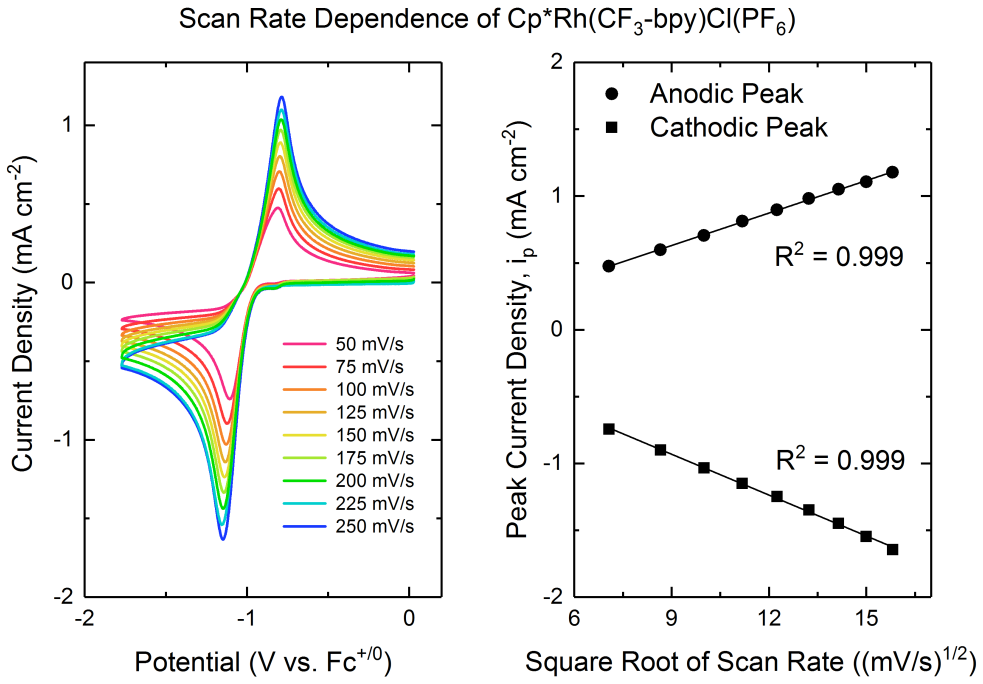

Figure 1.21: Scan rate dependence of **3,** illustrating a diffusional process.

With these electrochemical studies complete, we were interested in rationalizing the observed reduction potentials with the structures of the complexes. Such trends can be analyzed by considering the Hammett parameter. The Hammett parameter is generally utilized to explain the linear-free energy relationships for transformations involving substituted aromatic compounds; Hammett parameters have been tabulated based on the acid-base ionization of benzoic acids substituted by a given functional group or moiety.[18,19] The Hammett parameter, based on this experimental data, can be effectively used to describe the electron donating or electron withdrawing behaviors of a functional group, whether it be in the *ortho*-, *meta*-, or *para*-position, on benzoic acid. Although these parameters were originally developed for transformations involving benzoic acids, their usefulness extends to other molecules and other transformations involving substituted arenes. Here, we have adopted the Hammett parameter to gauge the relative electron donating and electron withdrawing properties of *para*-substituted bipyridine ligands, a similar conjugated, aromatic system. When we plot the reversible $Rh^{III/I}$ couples ($E_{1/2}$) for **1**, **2**, and **3** vs. the corresponding Hammett parameter we find a linear dependence (see Figure 1.22).

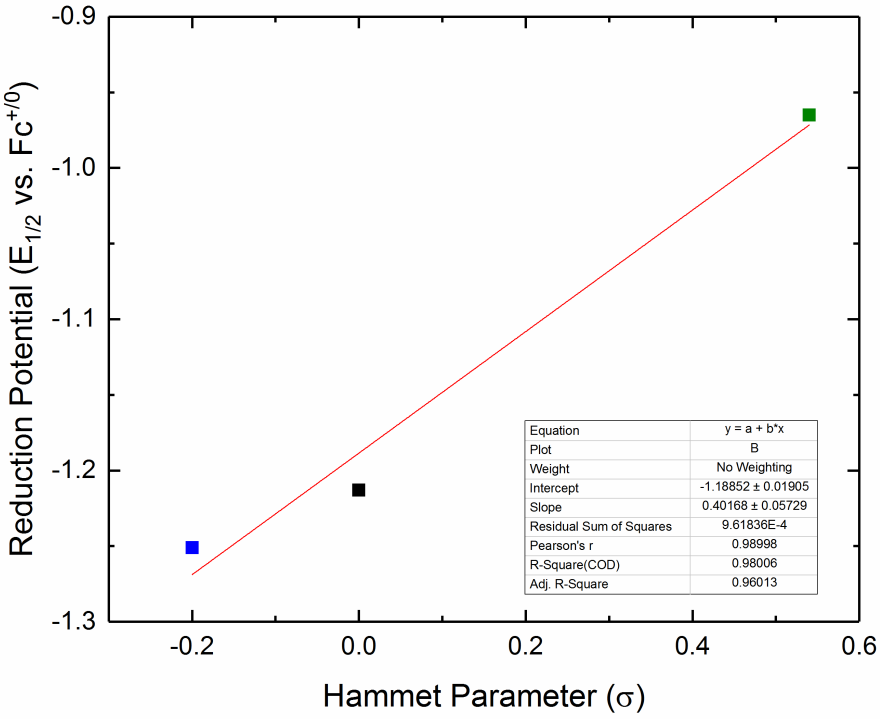

Figure 1.22: The standard reduction potential as a function of the Hammett parameter for **(blue)** $[Cp^*Rh(tBu\text{-}bpy)Cl]^+(PF_6)^-$, **(black)** $[Cp^*Rh(bpy)Cl]^+(PF_6)^-$, and **(green)** $[Cp^*Rh(CF_3\text{-}bpy)Cl]^+(PF_6)^-$.

This linear dependence suggests that the electronic properties of the ligand contribute to the electronic properties of the metal center. Complex **3**, bearing the CF_3-bpy ligand, has less reducing power for H_2 production and **1** has more reducing power. The possibility stands that during electrocatalysis the overpotential for these [Rh] complexes may be modulated based on how electron donating or electron withdrawing the bipyridine moiety is. These attractive findings present significant precedent to keep studying these model compounds, focusing primarily on electronic structure, to ultimately construct a better hydrogen evolution catalyst.

Electrochemistry: Cyclic Voltammetry with Acid Additions

The newly synthesized compounds, **1** and **3**, both exhibit a reversible $2e^-$ couple, similar to the parent compound, **2**, described by Grätzel. Given the observed similarities, acid addition experiments were performed to determine if the new complexes could also catalyze the input of protons and electrons to an output of hydrogen gas.[3] These experiments were carried out in an inert atmosphere glovebox where an electrochemical cell was equipped with a BPG working electrode, platinum counter electrode, and silver quasi-reference electrode. For this experiment, the Nernst equation needs to be satisfied under our chosen conditions; for us, this means use of a 1:1 mixture of anilinium triflate:aniline as the proton source, a temperature of 298 K, and operation of the electrochemical cell under 1 atm of H_2 gas (see equations 1.5-1.7). With these conditions established, we can directly calculate the reversible thermodynamic potential for proton-dihydrogen interconversion.

$$E_{H^+} = E^o_{H^+} + \frac{RT}{nF} ln \frac{[H^+]}{P_{H_2}} \quad (1.5)$$

$$E_{H^+} = E^o_{H^+} - 0.05916\,V \times pH \quad (1.6)$$

$$E_{H^+} = -0.028\,V - 0.05916\,V \times pH \quad (1.7)$$

In the above equations, $E_H{}^+$ is the equilibrium potential for the reduction of protons, $E^o{}_H{}^+$ is the half-cell reduction potential, R is the ideal gas constant, T is the temperature in Kelvin, n is the number of electrons transferred in the reaction, F is Faraday's constant, $[H^+]$ is the concentration of protons in the system, and P_{H2} is the pressure of hydrogen.[20]

Equation 1.6 results from rewriting equation 1.5 at standard temperature, 298 K, and one atmosphere of H_2. Equation 1.6 further simplifies to 1.7 when the experiment is carried out in MeCN vs. $Fc^{+/0}$.[20] The pKa then varies based on the choice of organic acid. The organic acid used for additions is added as a 1:1 mixture of acid and conjugate base, to satisfy the Henderson-Hasselbach equation, and subsequently the Nernst equation. Specifically, for this series of experiments, a 1:1 solution of anilinium triflate (pKa = 10.6 in MeCN) and aniline was used.[21] Since the variables of the Nernst equation are satisfied, E_H^+ can be estimated. The estimate of the reversible thermodynamic potential for the H^+/H_2 couple is determined to be –0.656 V vs. $Fc^{+/0}$ under our chosen conditions. With this information in hand, acid additions were made to solutions of complexes **1-3** and catalytic cyclic voltammetry experiments undertaken for each case (see Figures 1.23-1.25).

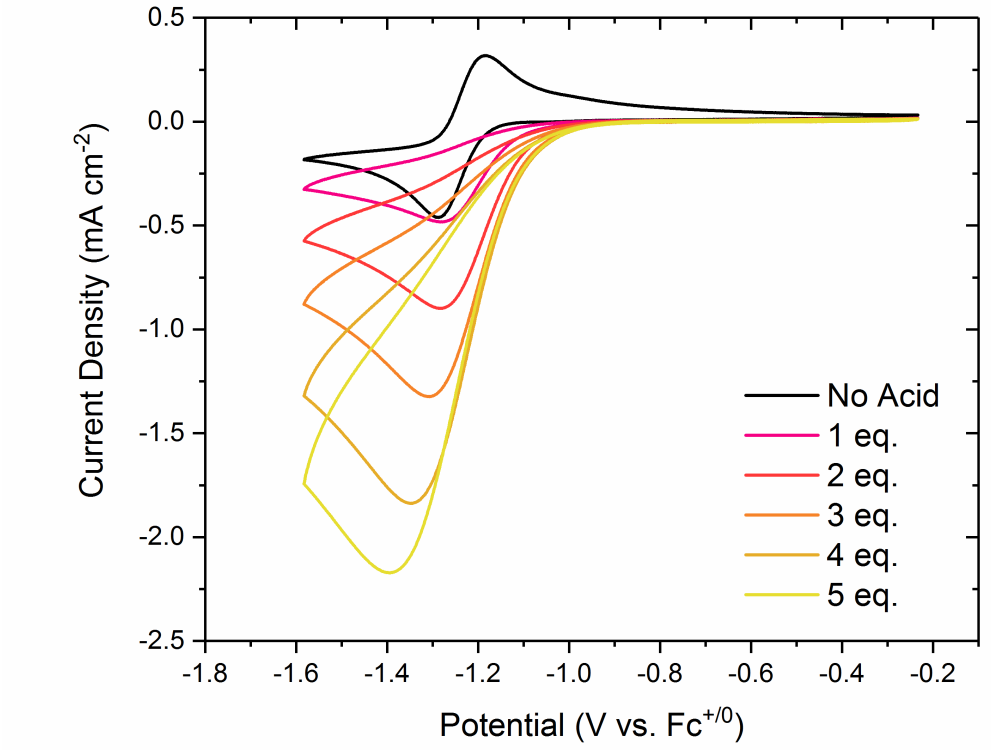

Figure 1.23: $[Cp^*Rh(tBu\text{-}bpy)Cl]^+(PF_6)^-$ with subsequent addition of anilinium triflate.

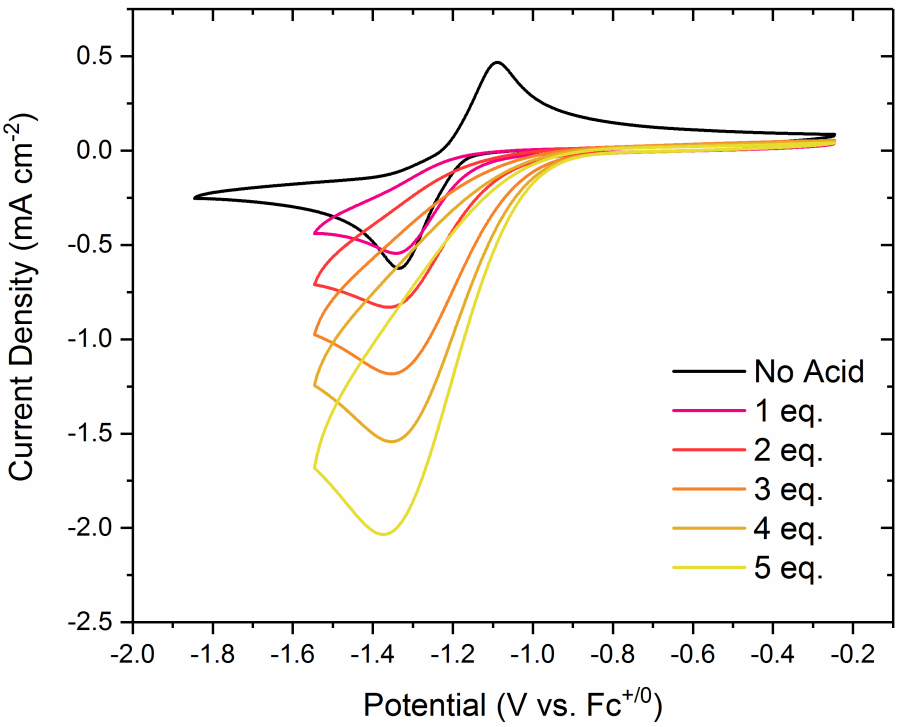

Figure 1.24: $[Cp^*Rh(bpy)Cl]^+(PF_6)^-$ with subsequent addition of anilinium triflate.

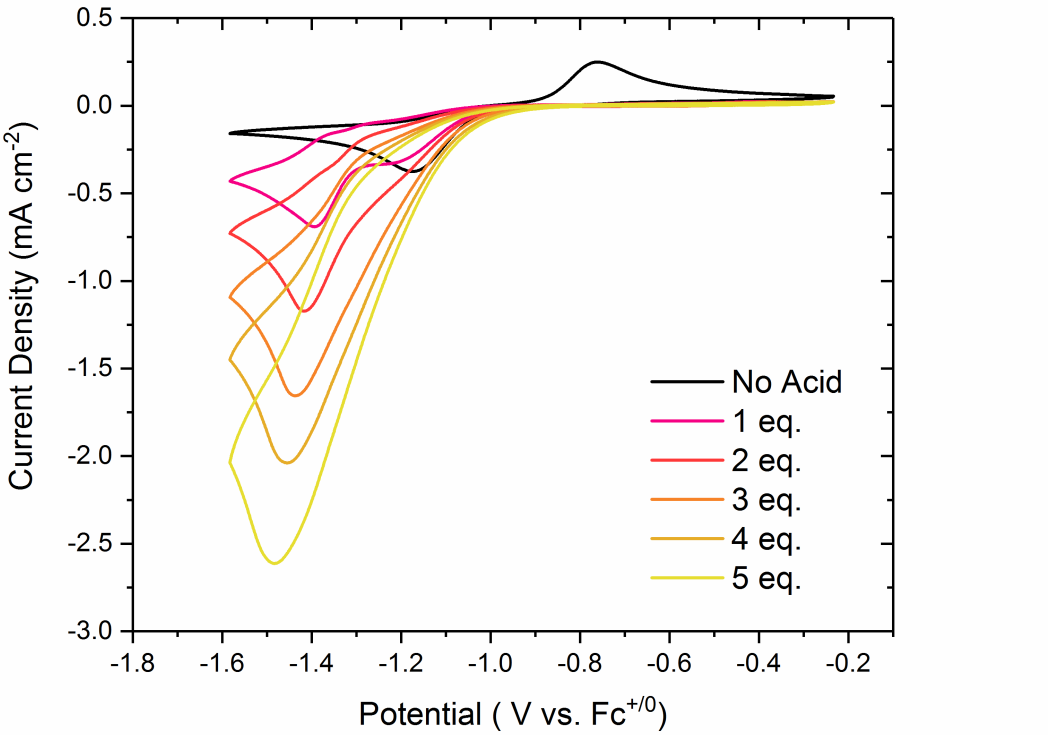

Figure 1.25: $[Cp^*Rh(CF_3\text{-bpy})Cl]^+(PF_6)^-$ with subsequent addition of anilinium triflate.

In each case, upon the addition of acid, we observe that the reversible behavior of the complex is lost, and a pseudocatalytic wave grows in. After one equivalent of acid is added to **3**, there are two observable reductions, a profile which is different when compared to complexes **1** and **2**. Both reductions show a gain in current density upon further addition of acid, suggesting that there are two species contributing to the evolution of hydrogen gas.

As more equivalents of acid are added we see the current density for each of the complexes increases as well. This is indicative of the ability of the catalyst to turnover substrate. Eventually, once sufficient excess acid is added, the catalytic activity becomes saturated, resulting in a plateauing effect of i_{cat}/i_p, where i_{cat} is the peak current for the irreversible catalytic wave observed in the presence of a given acid concentration and i_p is

the peak cathodic current for the complex in the absence of acid. Plotting i_{cat}/i_p as a function of proton concentration results in an observable plateau, suggesting a saturated kinetic regime has been reached (see Figures 1.26-1.28).

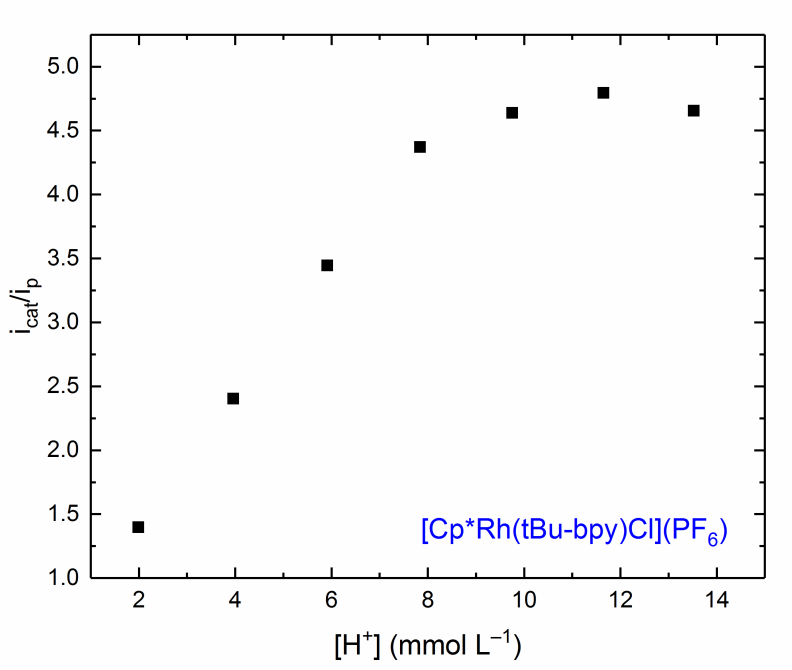

Figure 1.26: i_{cat}/i_p as a function of proton concentration for **1**, illustrating a plateau in the current enhancement.

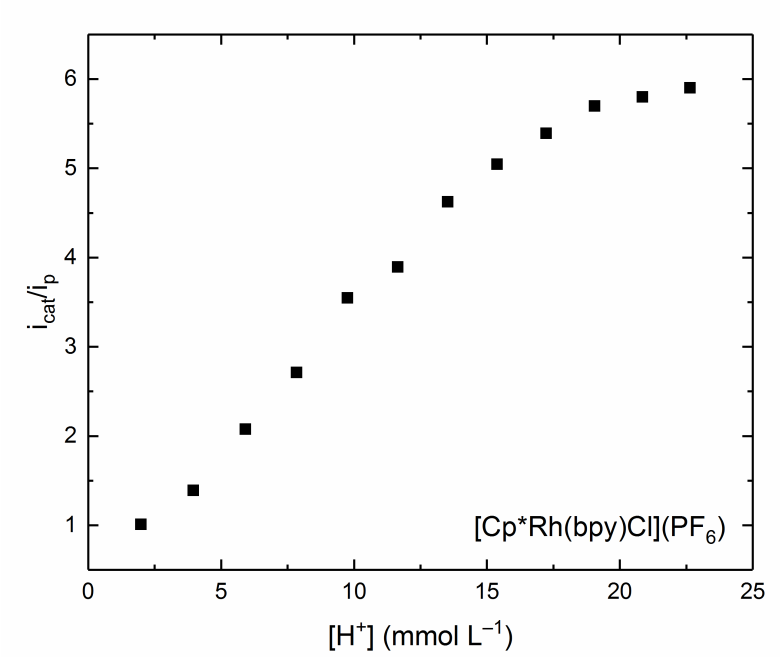

Figure 1.27: i_{cat}/i_p as a function of proton concentration for **2**, illustrating a plateau in the current enhancement.

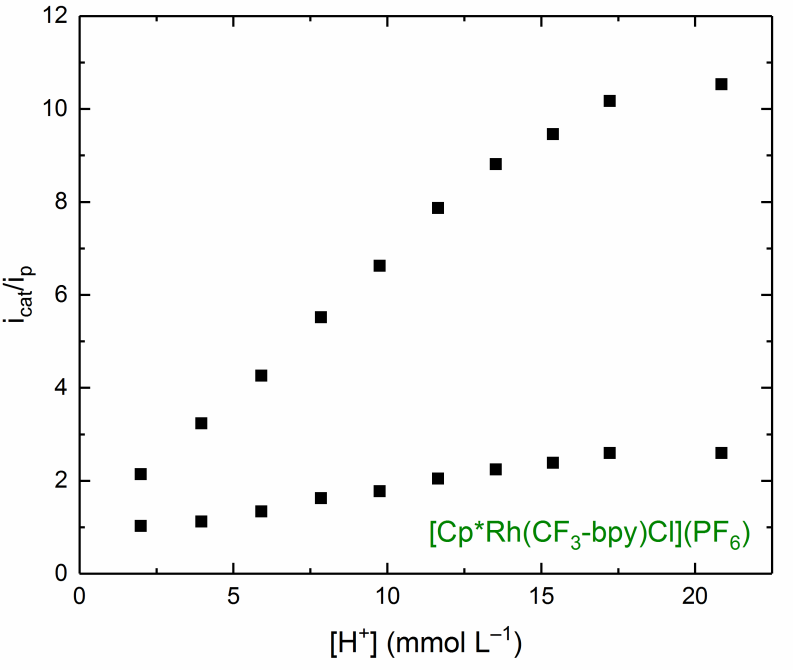

Figure 1.28: i_{cat}/i_p as a function of proton concentration for **3**, illustrating a plateau in the current enhancement.

Additionally, for each of the catalysts, we can estimate the potential for the onset of catalysis with 5 equiv. of anilinium triflate, under the above conditions.[2] The onset of catalysis is defined as half of the peak current for the irreversible catalytic wave observed in the presence of a given acid concentration ($E_{cat}/2$).[20] For **1**, the onset of catalysis occurs at −1.23 V, onset of catalysis for **2** occurs at −1.18 V, and the onset of catalysis for **3** occurs at −1.28 V. This corresponds to overpotentials of 569 mV, 519 mV, and 622 mV, respectively. Since enhancement occurred in the presence of acid, this suggests that hydrogen evolution is occurring and complexes **1-3** are candidate catalysts.

Bulk Electrolysis:

A bulk electrolysis was performed for complexes **1-3** to confirm their catalytic activity, and hydrogen (H_2) production via gas chromatography (GC) quantification and analysis of headspace gas. The cell consists of two chambers separated by a fine frit (see Figure 1.29).

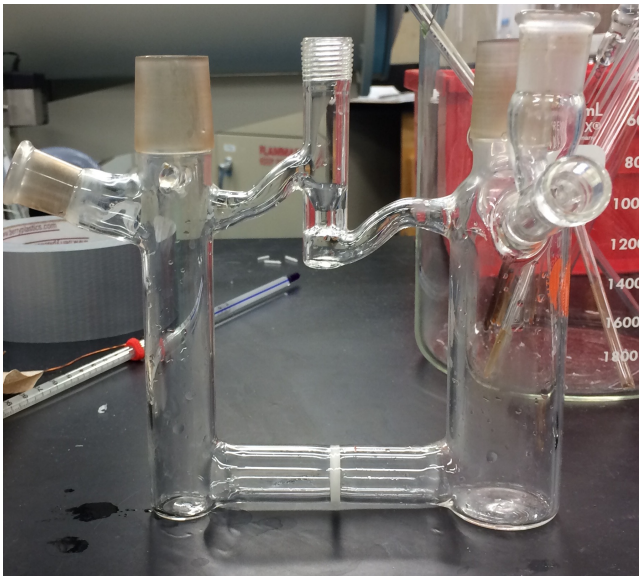

Figure 1.29: Cell used for electrolysis experiments; large chamber uses 38mL of electrolyte solution; small chamber uses 2o mL of electrolyte solution.

When the electrolysis cell is assembled, the cathodic (large) chamber consists of the catalyst, a proton source (anilinium triflate), a large BPG working electrode (10 cm^2), and a silver quasi reference electrode, while the anodic (small) chamber consists of an electron source and a platinum counter electrode (see Figure 1.30).

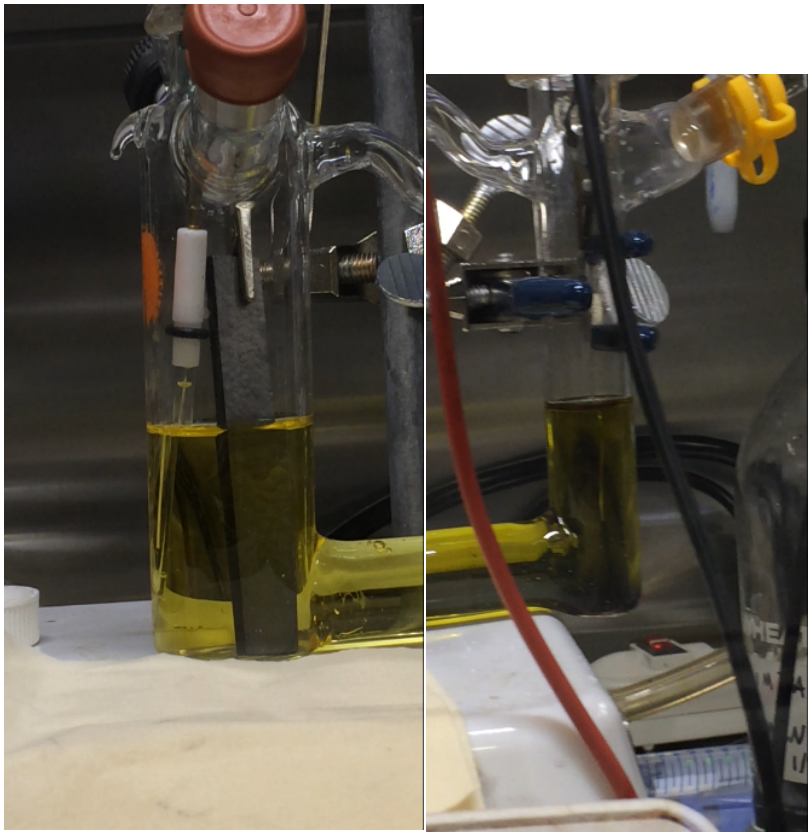

Figure 1.30: Carbon working electrode, silver reference electrode, catalyst, and anilinitum triflate (left). Platinum counter electrode and ferrocene (right).

For each of these experiments, the chemicals added to the bulk electrolysis cell consisted of 1 mM of catalyst and 10 mM of anilinium triflate in the large chamber, and 10 mM ferrocene, as a sacrificial electron source, in the small chamber. The overall reaction for this hydrogen-evolving bulk electrolysis can be expressed as a balanced chemical

equation leading to generation of hydrogen, free base, and ferrocenium triflate (see Scheme 1.4).

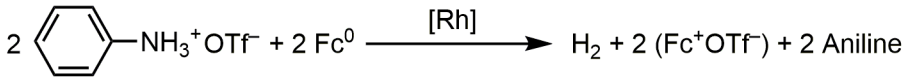

Scheme 1.4: Net reaction occurring during the bulk electrolysis of each [Rh] catalyst.

Each of the experiments were run at a controlled potential of -1.36 V vs. $Fc^{+/0}$ for 90 minutes. For the first 30 minutes of the electrolysis each of the compounds exhibit similar behavior. However, the systems pass differing amounts of current, which is indicative of different rates of catalysis (see Figure 1.31).

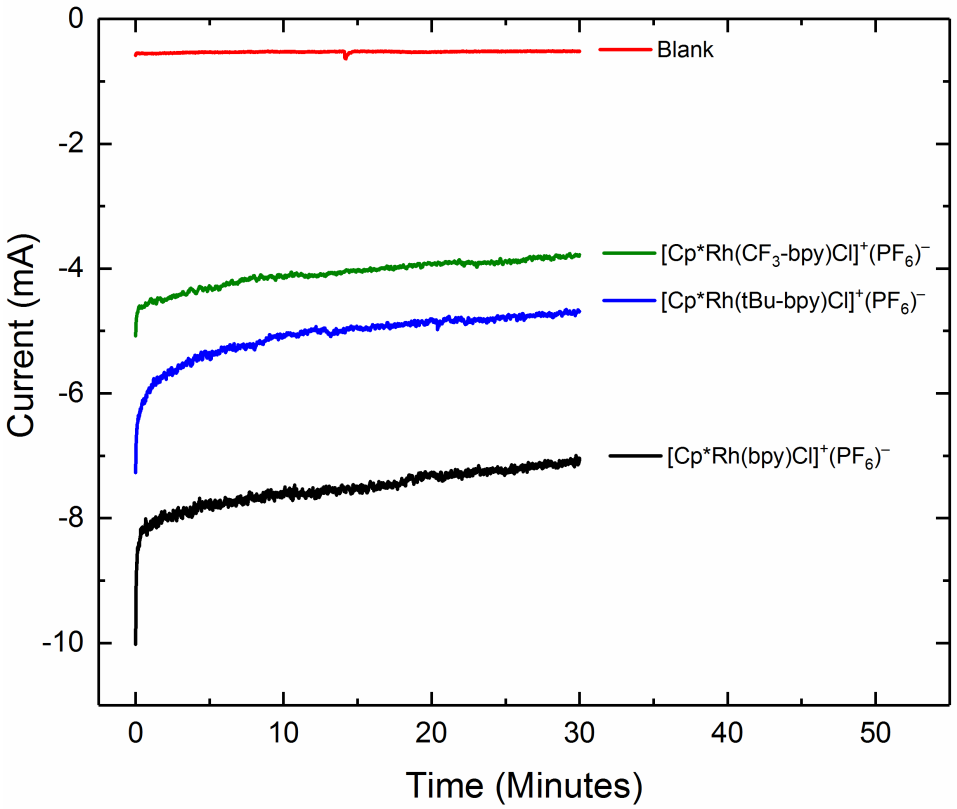

Figure 1.31: First 30 minutes of bulk electrolysis for each [Rh] complex.

In each of the electrolysis experiments, significantly more current is measured in the presence of the [Rh] catalyst compared to the bare BPG electrode (blank). Additionally, as the electrolysis experiments proceed through the 90-minute duration, the current observed for catalyst **2** begins to significantly decrease compared to the start of the experiment. This drop off can likely be attributed to the catalyst rapidly turning over protons and electrons to produce hydrogen. Since the substrate is being consumed more rapidly than in complexes **1** and **3**, we see a drop off in current due to lack of available free protons (see Figure 1.32).

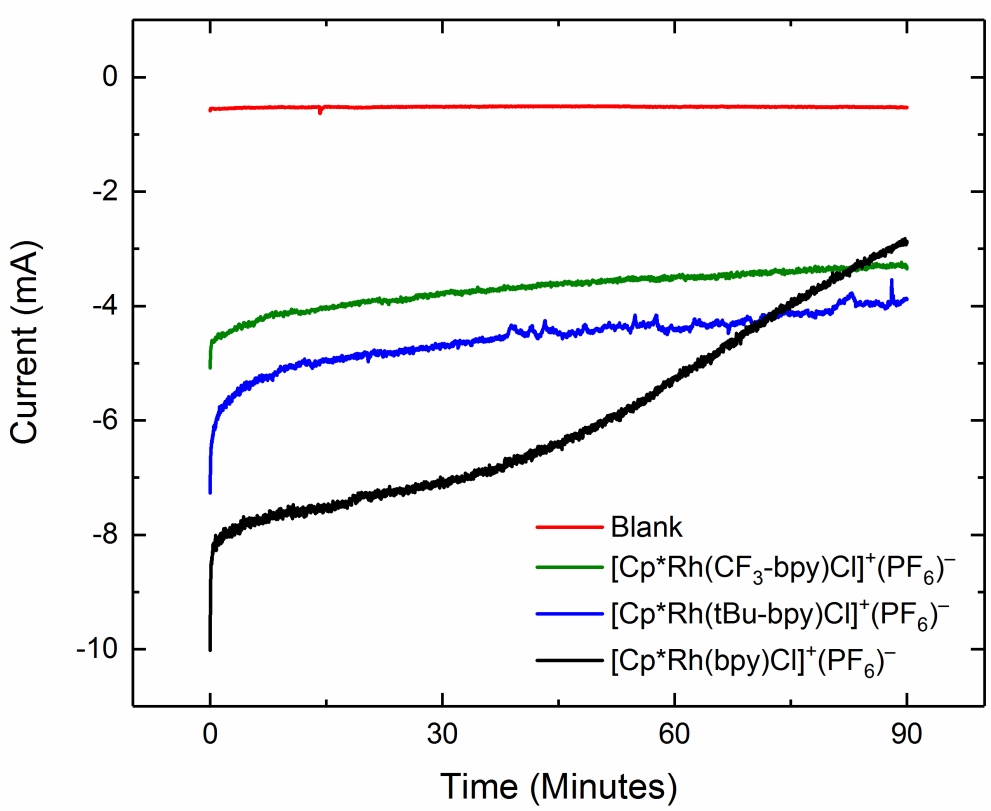

Figure 1.32: Controlled potential electrolysis for each [Rh] catalyst after 90 minutes.

We can also determine the amount of charge passed for each of the complexes during the electrolysis. The charge passed is used to calculate the theoretical amount of hydrogen that should have been produced at the end of the 90 minute experiment.

Following the 90 minute electrolysis, the headspace was immediately analyzed by GC. This confirms the actual amount of H_2 that is produced during the electrolysis. Here, we see that each complex has produced H_2 reconfirming the catalytic ability of **2** and confirming the catalytic capabilities of the newly synthesized complexes, **1** and **3** (see Figures 1.33-1.34)

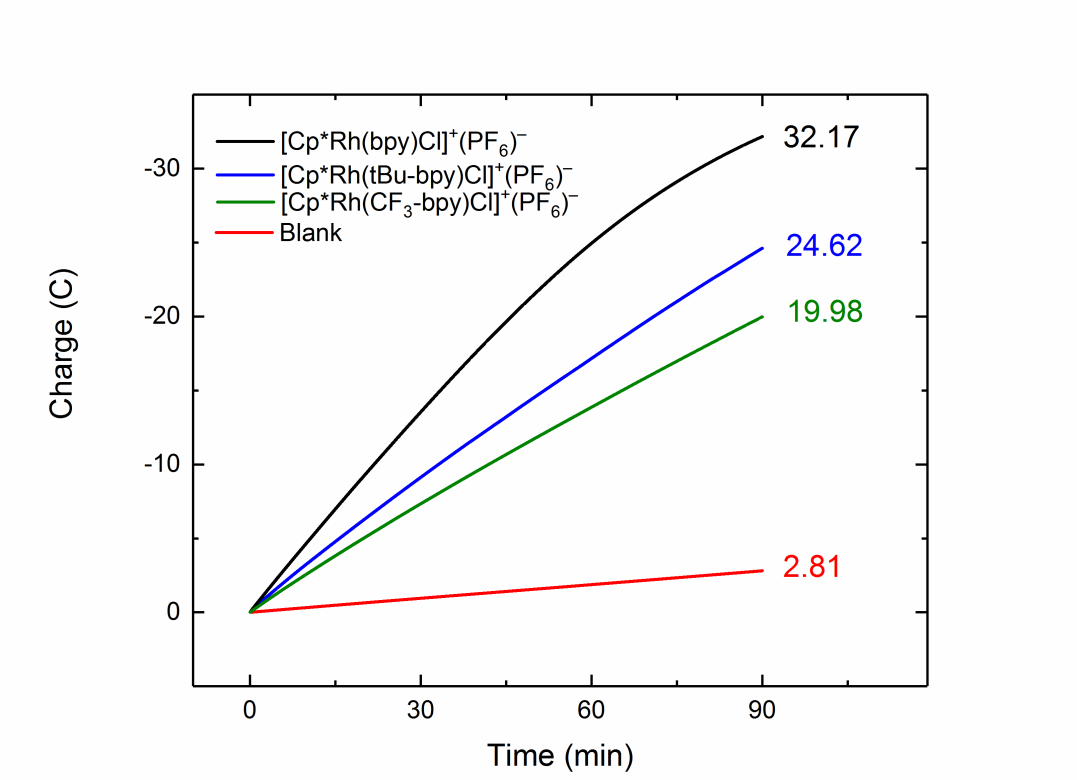

Figure 1.33: Charge plotted as a function of time; total charge passed included.

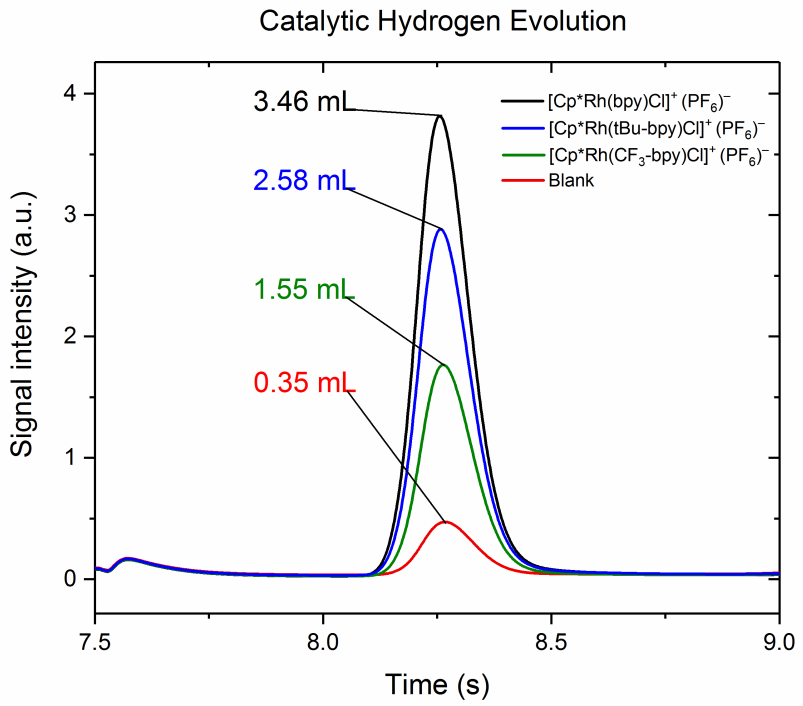

Figure 1.34: GC results confirming the different amounts hydrogen gas evolved among the different complexes.

The charge passed and catalytic evolution of hydrogen far exceed that of the bare carbon electrode (blank). From this data we can determine the turnover number and the Faradaic efficiency for each complex (see Table 1).

Compound	Amount of Hydrogen Detected (mL)	Faradaic Efficiency (±10%) (%)	Turn Over Number (TON)
[Rh(bpy)]	3.46	93	4.39
[Rh(CF_3-bpy)]	1.55	67	2.72
[Rh(tBu-bpy)]	2.58	90	3.36

Table 1: Faradaic efficiency and turnover number results for each complex following a 90 minute electrolysis in 0.1M $TBAPF_6$ in MeCN, with anilinium triflate as the proton source and Fc as the sacrificial reductant.

Enough ferrocene and anilinium triflate was added for a maximum of 5 turnovers, and all three catalysts were observed to have a TON greater than one. The previously reported catalyst, **2**, has a turnover number approaching the limit of five. This shows that the catalyst was indeed beginning to run out of substrate, likely attributing to the apparent current drop off during the electrolysis. Complexes **1** and **3** had lower turnover numbers, leading to the nearly steady current observed over the 90 minute electrolysis.

Complexes **1** and **2** have excellent Faradaic efficiencies. The Faradaic efficiency of **3** appears to be poor, but we suspected that this value was artificially low. We suspected formation of a secondary species, due to an obvious darkening of the electrolysis solution over the course of the experiment. This darkening occurred only in the case of **3**. The low apparent faradaic efficiency of **3** for H_2 production could be caused by misdirection of reducing equivalents from H_2 production to formation of another reduced compound that remains in solution. Specifically, once the $18e^-$ five-coordinate Cp*Rh(CF_3-bpy) complex forms upon $2e^-$ reduction. Because of the attenuated basicity of the reduced form of **3,** as judged by the reversible electrochemical studies, we hypothesized that this reduced form might require a further $1e^-$ reduction beyond the typical $2e^-$ process to give rise to a compound that is suitably electron rich to evolve H_2. This possibility would involve reduction of an intermediate [(Cp*H)Rh] compound; the starting material for such a reduction would be an $18e^-$ complex similar to that observed by Blakemore and Miller, namely $[(Cp^*H)Rh(CF_3\text{-bpy})NCMe]^+$. Specifically, Cp*Rh($CF_3$-bpy) could initially react with H^+ to form $[(Cp^*H)Rh(CF_3\text{-bpy})NCMe]^+$; this process is implicated by the loss of reversibility in the cyclic voltammetry upon additions of even small quantities of acid. The voltammetry carried out in the presence of acid, however, also shows growth of a

second, more negative reduction event. We propose that this reduction event corresponds to formation of a triply reduced compound, and that this triply reduced compound gives rise to an unexpected, additional electrocatalytic pathway.

To check this possibility, immediately following electrolysis, an aliquot of solution was examined from the cathodic chamber of the cell. The solvent from this sample was removed and a ^{1}H-NMR spectrum was collected for the remaining material. The ^{1}H-NMR spectrum revealed a new set of bipyridine signals in the aromatic region with resonances at 9.26 ppm (d, $^{3}J_{H\text{-}H}$ = 5.4Hz, 2H), 8.80 ppm (s, 2H), and 8.03 ppm (d, $^{3}J_{H\text{-}H}$ = 5.7 Hz, 2H) as well as a new doublet at 0.58 ppm (see Figures 1.35-1.36). This spectrum is highly reminiscent of that of (Cp*H)Rh(bpy)Br as synthesized by Blakemore.[8]

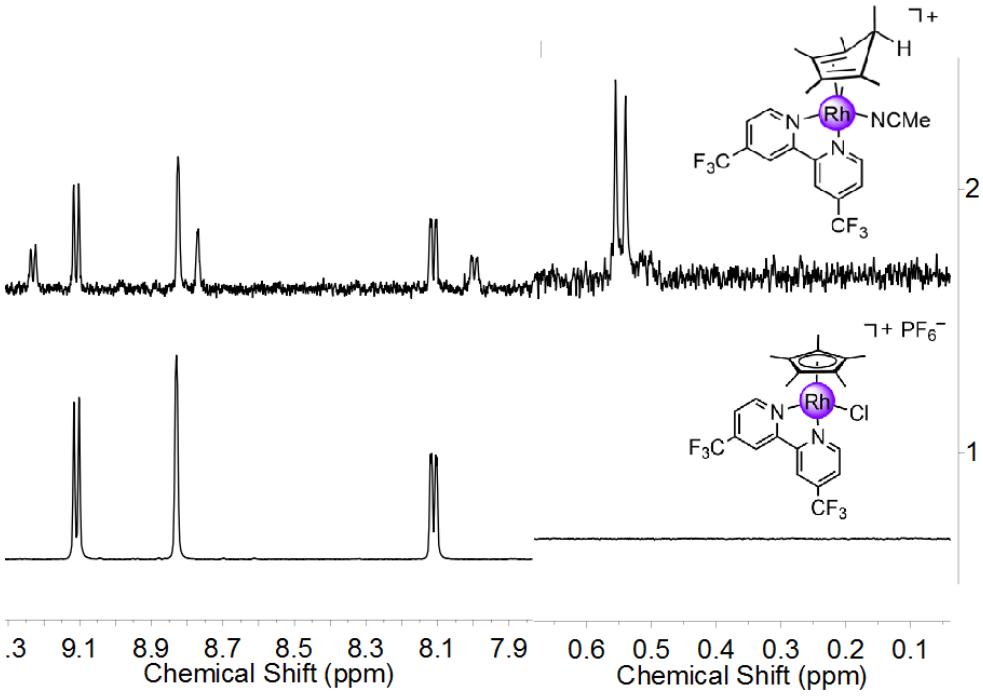

Figure 1.35: Comparison of starting material (bottom) to the isolated material (top) from the $[Cp^{*}Rh(CF_3\text{-bpy})Cl]^{+}(PF_6)^{-}$ bulk electrolysis .

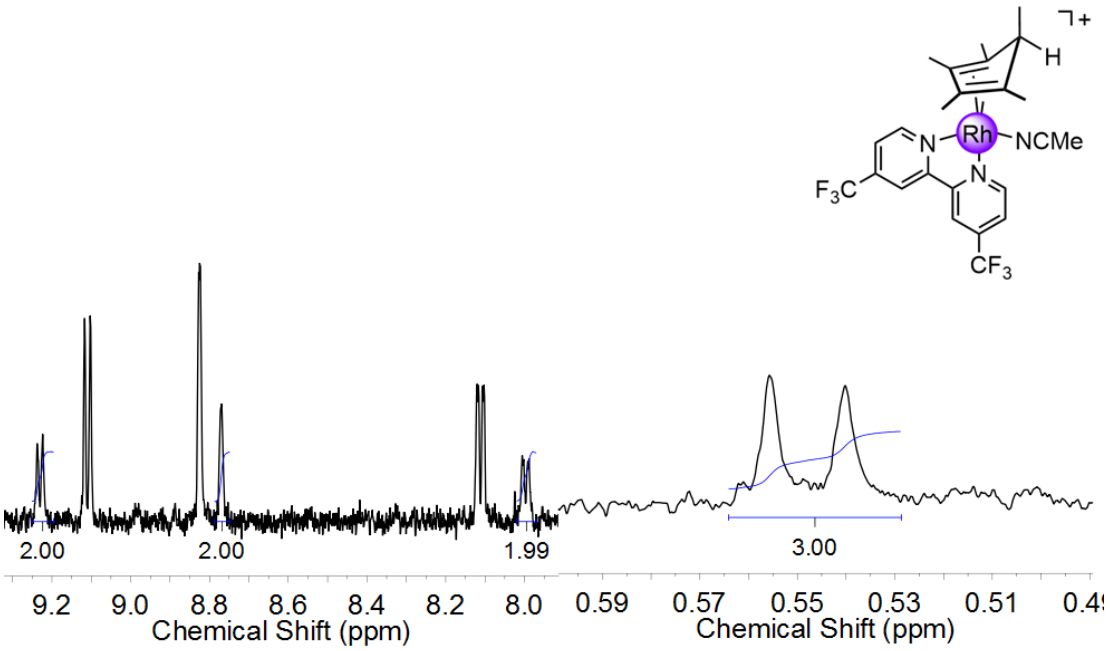

Figure 1.36: ^{1}H-NMR spectrum of material isolated from the cathodic chamber of the electrolysis cell. Integration of the isolated material and the proposed complex that is formed during bulk electrolysis.

Since a known concentration of **3** was put into the electrolysis cell and the isolated material is a representative sample, the available data can be used to calculate the amount of $[(Cp^*H)Rh(CF_3\text{-bpy})NCMe]^+$ produced in this experiment. A portion of the charge passed in the electrolysis is due to the production of this complex—this can be subtracted from the observed total charge passed to give the portion of charge passed that could have led to H_2 evolution. This amount of charge is the actual charge passed to generate hydrogen. Taking the $[(Cp^*H)Rh(CF_3\text{-bpy})NCMe]^+$ complex into consideration, the Faradaic efficiency increases to a respectable and reasonable 93%. We note, however, that to fully confirm this proposal, the $[(Cp^*H)Rh(CF_3\text{-bpy})NCMe]^+$ complex must be prepared and then compared to the material observed in the electrolysis aliquot. This effort is currently underway.

The electrochemical response of **3** upon addition of acid was distinct from complexes **1** and **2**. When one equivalent of acid is added, we see current enhancement for two reductions, and both are irreversible waves. This suggests a different reaction pathway occurring, compared to **1** and **2**. Notably, no [(Cp*H)Rh] complexes were observed following electrolyses of **1** or **2**. To explain this in more detail, we will start with consideration of the two pathways of hydrogen evolution collectively proposed by Grätzel and Blakemore (see Schemes 1.5-1.6).

$$[Cp^*Rh(bpy)] + H^+ \longrightarrow [Cp^*Rh(bpy)H]^+$$

$$[Cp^*Rh(bpy)H]^+ + H^+ \longrightarrow [Cp^*Rh(bpy)NCMe]^{2+} + H_2$$

Scheme 1.5: Hydrogen evolution pathway proposed by Grätzel.

$$[Cp^*Rh(bpy)] + H^+ \longrightarrow [(Cp^*H)Rh(bpy)NCMe]^+$$

$$[(Cp^*H)Rh(bpy)NCMe]^+ + H^+ \longrightarrow [Cp^*Rh(bpy)NCMe]^{2+} + H_2$$

Scheme 1.6: Hydrogen evolution pathway proposed by Blakemore.

Grätzel's pathway favors formation of a rhodium hydride species upon reaction of the reduced complex with one equivalent of acid, and hydrogen evolution after reaction with a second equivalent of acid. In a somewhat similar sequence, Blakemore's pathway suggests that when acid is added, a [(Cp*H)Rh] species is produced and upon further addition of acid the compound can evolve hydrogen. The observation of [(Cp*H)Rh(CF_3-bpy)NCMe]$^+$ and the absence of the similar tBu-bpy and bpy analogues suggests that the

trifluoromethyl substituents make the Cp*H complex too stable, and the pathways to hydrogen evolution seem to have changed. A stronger acid or slightly more negative voltage may be needed to access further reduction. In accord with these general consideration, we have isolated a significant amount of $[(Cp^*H)Rh(CF_3\text{-bpy})NCMe]^+$ from a post-electrolysis solution that contains excess acid. This isolation strongly suggests that the isolated $[(Cp^*H)Rh(CF_3\text{-bpy})NCMe]^+$ material is not sufficiently basic to take up a second equivalent of acid and evolve hydrogen. Thus, our experimental work implicates a new and previously unknown catalytic pathway that involves a further reduction of $[(Cp^*H)Rh(CF_3\text{-bpy})NCMe]^+$ to generate a compound that is sufficiently basic to react with acid (see Scheme 1.7).

$$[(Cp^*H)Rh(CF_3\text{-bpy})NCMe]^+ \xrightarrow{+e^-} [(Cp^*H)Rh(CF_3\text{-bpy}^{\bullet -})NCMe]$$

$$[(Cp^*H)Rh(CF_3\text{-bpy}^{\bullet -})NCMe] + H^+ \longrightarrow [Cp^*Rh(CF_3\text{-bpy})NCMe]^+ + H_2$$

$$[Cp^*Rh(CF_3\text{-bpy})NCMe]^+ \longrightarrow 1/2[Cp^*Rh(CF_3\text{-bpy})NCMe]^{2+} + 1/2[Cp^*Rh(CF_3\text{-bpy})]$$

Scheme 1.7: Possible third catalytic pathway, mediated through Cp*H.

Here, once the $[(Cp^*H)Rh(CF_3\text{-bpy})NCMe]^+$ complex is formed, a third electron can be introduced into the system. Indeed, this compound would be predicted to be susceptible to reduction at a fairly modest potential, as reduction could generate a metal-ligated, CF_3-bpy-centered anion radical. Such a species is attractive in that delocalization of the additional electron density around the bipyridine ring is possible, in addition to stabilization afforded by the presence of trifluoromethyl substituents on the bpy system. In the presence of acid, this complex would likely evolve hydrogen upon formation. Following H_2 generation, the rhodium product would be a formally $[Rh^{II}]$ species. Such a

[Rh^{II}] species is known to be unstable in this system—evidence for this is clear from the clean, 2e– electrochemistry in the absence of acid. Stated another way, the potential for reduction of Rh^{III} to Rh^{II} in this system is more negative than for the reduction of Rh^{II} to Rh^{I}. Thus, generation of Rh^{II} would result in a disproportionation reaction that produces half an equivalent of $[Cp^*Rh(CF_3\text{-bpy})NCMe]^{2+}$ and $[Cp^*Rh(CF_3\text{-bpy})]$. In accord with the involvement of such a reaction sequence here, we only detect $[Cp^*Rh(CF_3\text{-bpy})NCMe]^{2+}$ and $[(Cp^*H)Rh(CF_3\text{-bpy})NCMe]^{+}$ following electrolysis. The amount of $[Cp^*Rh(CF_3\text{-bpy})]$ produced in the final disproportionation step would be rapidly consumed by protonation with remaining acid present in the system to generate $[(Cp^*H)Rh(CF_3\text{-bpy})NCMe]^{+}$ which is metastable under the conditions present in this electrocatalytic system.

Conclusions

This thesis describes the synthesis, characterization, and electrochemical studies of two new rhodium-based hydrogen evolution catalysts. We have confirmed catalytic activity of two new derivatives, **1** and **3**, and compared them to the parent complex, **2**. For both new catalysts, the overpotential is higher and the turnover number is lower, but the Faradaic efficiency remains high. Thus, our efforts have yielded active catalysts. Although they are not as efficient as the parent system, we have gained valuable insight into how ligand substitutions can modulate catalytic activity in this family of complexes. Generally, these studies reveal that the parent [Cp*Rh(bpy)] system displays ideal electronic coupling between the metal and its non-innocent ligands to afford a highly active catalyst. Complex **3** provides a crucial insight to a rarely observed intermediate and implicates the possibility of a third catalytic pathway in hydrogen evolution with

these complexes—this pathway involves $[(Cp^*H)Rh(CF_3\text{-}bpy)NCMe]^+$. Future studies will focus on the goal of synthesizing, isolating, and characterizing this material for use in kinetic and mechanistic investigations.

R e f e r e n c e s

[1]Lewis, N. S.; Nocera, D. G., Powering the planet: Chemical challenges in solar energy utilization. *Proc. Nat. Acad. Sci. U.S.A.* **2006,** *103*, 15729-15735.

[2]Laga, Stephanie. "A tale of two cobalts." *Caltech Thesis.* June 16, **2014**. http://thesis.library.caltech.edu/8244/ (accessed April 3, 2017).

[3]Michael Grätzel, U. K., Electrochemical and Pulseradiolytic Reduction of (Pentamethyl-cyclopentadienyl(polypyridyl)rhodium Complexes. *Chem. Ber.* **1989,** *122*, 1869-1880.

[4] Chardon-Noblat, S.; Cosnier, S.; Deronzier, A.; Vlachopoulos, N., Electrochemical properties of [(C5Me5)RhIII(L)Cl]+ complexes (L = 2,2′-bipyridine or 1,10-phenanthroline derivatives) in solution in related polypyrrolic films. Application to electrocatalytic hydrogen generation. *J. Electroanal. Chem.* **1993,** *352*, 213-228.

[5] Singh, S. K.; Trivedi, M.; Chandra, M.; Pandey, D. S., Rhodium(III) pentamethyl cyclopentadienyl complexes incorporating 1-(4-cyanophenyl)-imidazole: role of solvent in ligand substitution reactions. *J. Organomet. Chem.* **2005,** *690*, 647-652.

[6] Blakemore, J. D.; Gupta, A.; Warren, J. J.; Brunschwig, B. S.; Gray, H. B., Noncovalent Immobilization of Electrocatalysts on Carbon Electrodes for Fuel Production. *J. Am. Chem. Soc.* **2013,** *135*, 18288-18291.

[7] Blakemore, J. D.; Hernandez, E. S.; Sattler, W.; Hunter, B. M.; Henling, L. M.; Brunschwig, B. S.; Gray, H. B., Pentamethylcyclopentadienyl rhodium complexes. *Polyhedron* **2014,** *84*, 14-18.

[8] Quintana, L. M. A.; Johnson, S. I.; Corona, S. L.; Villatoro, W.; Goddard, W. A.; Takase, M. K.; VanderVelde, D. G.; Winkler, J. R.; Gray, H. B.; Blakemore, J. D., Proton–hydride tautomerism in hydrogen evolution catalysis. *Proc. of the Natl. Acad. Sci. U.S.A.* **2016,** *113*, 6409-6414.

[9] Pitman, C. L.; Finster, O. N. L.; Miller, A. J. M., Cyclopentadiene-mediated hydride transfer from rhodium complexes. *Chem. Commun.* **2016,** *52*, 9105-9108.

[10] Pangborn, A. B.; Giardello, M. A.; Grubbs, R. H.; Rosen, R. K.; Timmers, F. J., Safe and Convenient Procedure for Solvent Purification. *Organometallics* **1996,** *15*, 1518-1520.

[11] White, C.; Yates, A.; Maitlis, P. M.; Heinekey, D. M., (η5-Pentamethylcyclopentadienyl)Rhodium and -Iridium Compounds. In *Inorg. Synth.*, John Wiley & Sons, Inc.: 2007; pp 228-234.

[12] Ritter, K.; Pehlken, C.; Sorsche, D.; Rau, S., Optimized synthesis of a tert-butyl-phenyl-substituted tetrapyridophenazine ligand and its Ru(ii) complexes and determination of dimerization behaviour of the complexes through supramolecular "Fingerhakel". *Dalton Trans.* **2015,** *44*, 8889-8905.

[13] Li, H.; Oppenheimer, J.; Smith Iii, M. R.; Maleczka Jr, R. E., Improved synthesis of electron deficient bipyridines. *Tetrahedron Lett.* **2016,** *57*, 2231-2232.

[14] Bodenhausen, G.; Ruben, D. J., Natural abundance nitrogen-15 NMR by enhanced heteronuclear spectroscopy. *Chem. Phys. Lett.* **1980,** *69*, 185-189.

[15] Smith, Jancice Gorzynski, *Organic Chemistry*. McGraw-Hill Education, New York, New York, **2008**.

[16] Scharwitz, M. A.; Ott, I.; Geldmacher, Y.; Gust, R.; Sheldrick, W. S., Cytotoxic half-sandwich rhodium(III) complexes: Polypyridyl ligand influence on their DNA binding properties and cellular uptake. *J. Organomet. Chem.* **2008,** *693*, 2299-2309.

[17]Bard, A. J., *Electrochemical Methods: Fundamentals and Applications*. Wiley: New York, **2001**; Vol. 2.

[18] Hammett, L. P., The Effect of Structure upon the Reactions of Organic Compounds. Benzene Derivatives. *J. Am. Chem. Soc.* **1937,** *59*, 96-103.

[19] Hansch, C.; Leo, A.; Taft, R. W., A survey of Hammett substituent constants and resonance and field parameters. *Chem. Rev.* **1991,** *91*, 165-195.

[20] Appel, A. M.; Helm, M. L., Determining the Overpotential for a Molecular Electrocatalyst. *ACS Catal.* **2014,** *4*, 630-633.

[21] Muckerman, J. T.; Skone, J. H.; Ning, M.; Wasada-Tsutsui, Y., Toward the accurate calculation of pKa values in water and acetonitrile. *Biochem. Biophys. Acta. – Bioenerg.* **2013,** *1827*, 882-891.

[22] Fulmer, G. R.; Miller, A. J. M.; Sherden, N. H.; Gottlieb, H. E.; Nudelman, A.; Stoltz, B. M.; Bercaw, J. E.; Goldberg, K. I., NMR Chemical Shifts of Trace Impurities: Common Laboratory Solvents, Organics, and Gases in Deuterated Solvents Relevant to the Organometallic Chemist. *Organometallics* **2010,** *29*, 2176-2179.

A p p e n d i x A

CHAPTER 1 SUPPORTING INFORMATION

Experimental Methods

General. All solvents were of commercial grade and dried over activated alumina using a Grubbs-type solvent purification system prior to use.[10] ^{1}H, ^{13}C, ^{19}F, ^{31}P, and HSQC NMR spectra were collected on 400 and 500 MHz Bruker spectrometers and referenced to the residual protio-solvent signal in case of ^{1}H and ^{13}C or the deuterium lock signal in the case of ^{19}F and ^{31}P.[22] Chemical shifts (δ) are reported in units of ppm and coupling constants (*J*) are reported in Hz. Gas chromatography data was collected using a Shimadzu GC-2014 consisting of a thermal conductivity detector and dual flame-ionization detectors. Mass spectrometry data was collected on an Electrospray Micromass LCT Premier mass spectrometer. Single-crystal diffraction data were collected with a Bruker KAPPA APEX-II X-ray diffractometer. Electrochemical measurements were made in an inert atmosphere glovebox using a Gamry Reference 600+ potentiostat. The electrolyte for each experiment was 0.1 M electrochemical grade *N*-tetrabutylamonium hexafluorophosphate in MeCN. A three-electrode system is utilized, comprised of a basal plane of highly oriented pyrolytic graphite working electrode (surface area 0.09 cm^2), a platinum counter electrode, and a Ag/Ag^+ reference electrode along with a $Fc^{+/0}$ as an external reference.

[(η^5-C_5Me_5)Rh(4,4′-di-*tert*-butyl-2,2′-bipyridine)Cl](PF_6)

To a 20mL scintillation vial equipped with a Teflon stir bar, $[Cp^*RhCl_2]_2$ was dissolved in MeCN (ca. 4mL) to give a deep red solution. To this solution, $AgPF_6$ in MeCN (ca.

2mL) was added resulting in a lightening of the red solution to orange with AgCl as a precipitate. The solution was allowed to stir for 10 min. Then the tBu-bpy ligand was dissolved in THF (ca. 2mL) and was added to the orange solution. Upon addition, the solution lightens to a sunny-yellow and is allowed to stir for 15 min. The AgCl was then filtered off and the resulting yellow solution in the filter flask was placed in a scintillation vial and solution diluted with diethyl ether to precipitate the desired product. The yellow solid was then filtered to afford [(η^5-C_5Me_5)Rh(4,4′-di-*tert*-butyl-2,2′-bipyridine)Cl](PF_6). ^{1}H NMR (400 MHz, CD_3CN) δ 8.77 [d, $^3J_{H\text{-}H}$ = 6.0 Hz, 2H, (Me_5C_5)Rh($C_{18}H_{24}N_2$)], 8.39 [d, $^4J_{H\text{-}H}$ = 2.0 Hz, 2H, (Me_5C_5)Rh($C_{18}H_{24}N_2$)], 7.80 [dd, $^3J_{H\text{-}H}$ = 6.0 Hz, $^4J_{H\text{-}H}$ = 2.1 Hz, 2H, (Me_5C_5)Rh($C_{18}H_{24}N_2$)], 1.68 [s, 15H, (Me_5C_5)Rh($C_{18}H_{24}N_2$)], 1.48 [s, 18H, (Me_5C_5)Rh($C_{18}H_{24}N_2$)] ppm. ^{13}C{^{1}H} NMR (126MHz, CD_3CN) δ 165.6[s, 2C, (Me_5C_5)Rh($C_{18}H_{24}N_2$)], 154.8 [s, 2C, (Me_5C_5)Rh($C_{18}H_{24}N_2$)], 152.0 [s, 2C, (Me_5C_5)Rh($C_{18}H_{24}N_2$)], 125.9 [s, 2C, (Me_5C_5)Rh($C_{18}H_{24}N_2$)], 121.6 [s, 2C, (Me_5C_5)Rh($C_{18}H_{24}N_2$)], 97.6 [d, $^1J_{Rh\text{-}C}$ =8.2 Hz, 5C, (Me_5C_5)Rh($C_{18}H_{24}N_2$)], 36.1 [s, 2C, (Me_5C_5)Rh($C_{18}H_{24}N_2$)], 30.0 [s, 6C, (Me_5C_5)Rh($C_{18}H_{24}N_2$)], 8.7 [s, 5C, (Me_5C_5)Rh($C_{18}H_{24}N_2$)] ppm. ESI-MS (positive) m/z: found 541.1 m/z (100%) (**1**-PF_6^-), 542.1 m/z (31%), 543.1 (37%), 544.1 (11%).

[(η^5-C_5Me_5)Rh(4,4′-bis(trifluoromethyl) -2,2′-bipyridine)Cl](PF_6)

To a 20mL scintillation vial equipped with a Teflon stir bar, [Cp*$RhCl_2$]$_2$ was dissolved in MeCN (ca. 4mL) to give a deep red solution. To this solution, $AgPF_6$ in MeCN (ca. 2mL) was added resulting in a lightening of the red solution to orange with AgCl as a precipitate. Then the CF_3-bpy ligand was dissolved in MeCN (ca. 2mL) and was added

to the orange solution. Upon addition, the solution lightens to a sunny-yellow and is allowed to stir for 15 min. The AgCl was then filtered off and the resulting yellow solution in the filter flask was placed in a scintillation vial and solution diluted with diethyl ether to precipitate the desired product. The yellow solid was then filtered to afford [(η^5-C_5Me_5)Rh(4,4′-bis-trifluoromethyl-2,2′-bipyridine)Cl](PF_6) (). ^{1}H NMR (400 MHz, CD_3CN) δ 9.14 (d, $^3J_{H-H}$ = 5.8 Hz, 2H, (Me_5C_5)Rh($C_{12}H_6F_6N_2$)], 8.86 [d, $^4J_{H-H}$ = 1.7 Hz, 2H, (Me_5C_5)Rh($C_{12}H_6F_6N_2$)], 8.14 (dd, $^3J_{H-H}$ = 5.8 Hz, $^4J_{H-H}$ = 1.3 Hz, 2H, (Me_5C_5)Rh($C_{12}H_6F_6N_2$)], 1.71 (s, 15H, (Me_5C_5)Rh($C_{12}H_6F_6N_2$)] ppm. $^{13}C\{^1H\}$ NMR (126MHz, CD_3CN) δ 155.2 (s, 2C, (Me_5C_5)Rh($C_{12}H_6F_6N_2$)], 154.0 (s, 2C, (Me_5C_5)Rh($C_{12}H_6F_6N_2$)], 141.5 (q, $^1J_{C-F}$ = 35.6 Hz, 2C, (Me_5C_5)Rh($C_{12}H_6F_6N_2$)], 125.3 (q, $^4J_{C-F}$ = 3.5 Hz, 2C, (Me_5C_5)Rh($C_{12}H_6F_6N_2$)], 123.8 (s, 2C, (Me_5C_5)Rh($C_{12}H_6F_6N_2$)], 121.6 (q, $^4J_{C-F}$ = 3.5 Hz, 2C, (Me_5C_5)Rh($C_{12}H_6F_6N_2$)], 98.2 (d, $^1J_{Rh-C}$ = 8.2 Hz, 5C, (Me_5C_5)Rh($C_{12}H_6F_6N_2$)], 8.8 (s, 5C, (Me_5C_5)Rh($C_{12}H_6F_6N_2$)] ppm. ^{19}F NMR (376 MHz, CD_3CN) δ -65.4 (s, 6F, (Me_5C_5)Rh($C_{18}H_{24}N_2$)] ppm. ESI-MS (positive) m/z: found 565.0 m/z (100%) (**1**-PF_6^-), 566.0 m/z (75%), 567.0 (95%), 568.0 (21%).

Acid-Only Electrochemistry Background Data

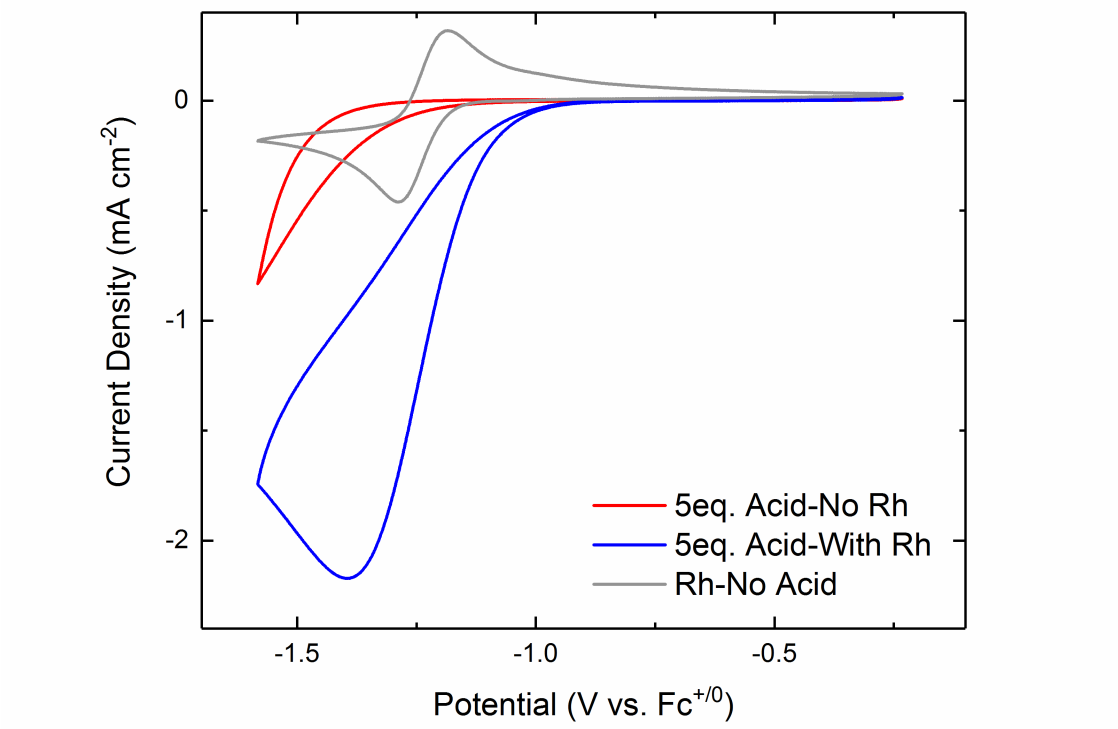

Figure A1: Comparing the differences in current density between the bare electrode and when the catalyst is present at 5eq. of acid, for $[Cp^*Rh(tBu\text{-}bpy)Cl]^+(PF_6)^-$.

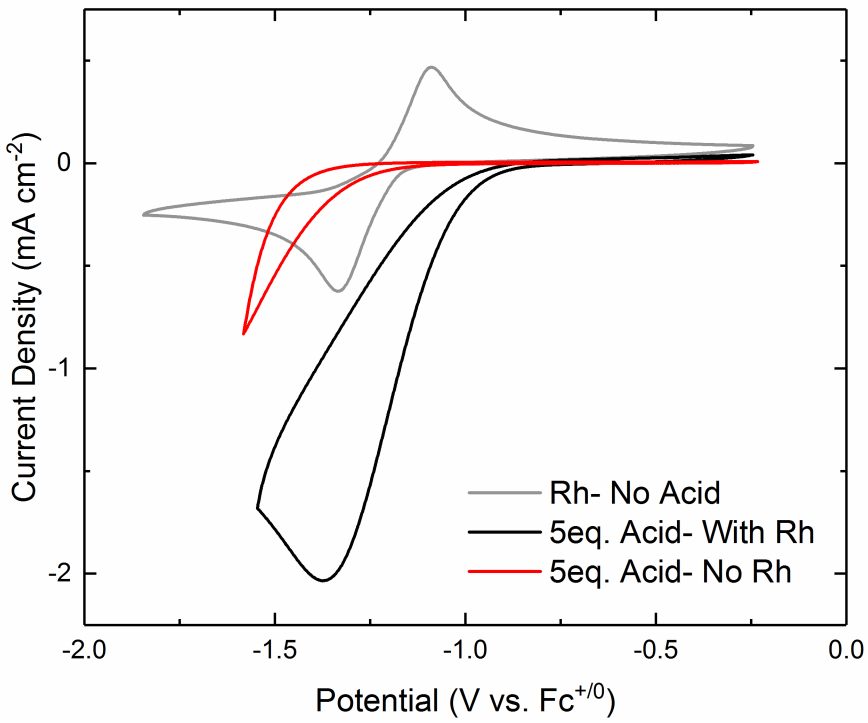

Figure A2: Comparing the differences in current density between the bare electrode and when the catalyst is present at 5eq. of acid, for $[Cp^*Rh(bpy)Cl]^+(PF_6)^-$.

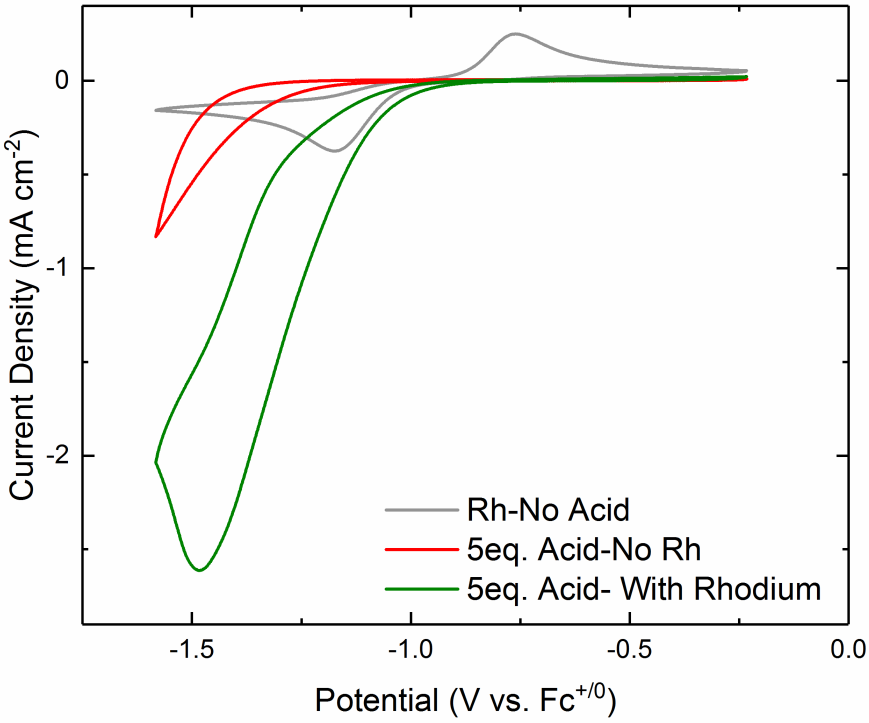

Figure A3: Comparing the differences in current density between the bare electrode and when the catalyst is present at 5eq. of acid, for $[Cp^*Rh(CF_3\text{-bpy})Cl]^+(PF_6)^-$.

^{1}H-NMR Spectra of Isolated Material from Bulk Electrolysis

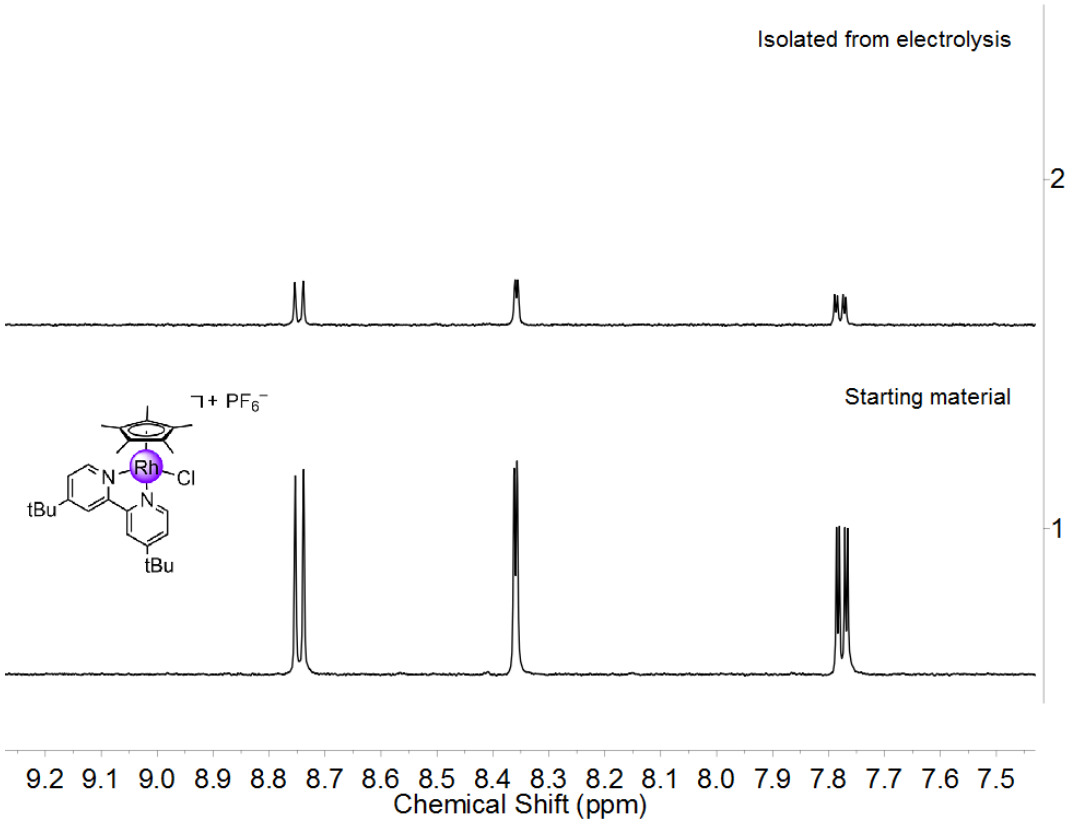

Figure A4: Isolated material from the bulk electrolysis of **1** compared to the starting material.

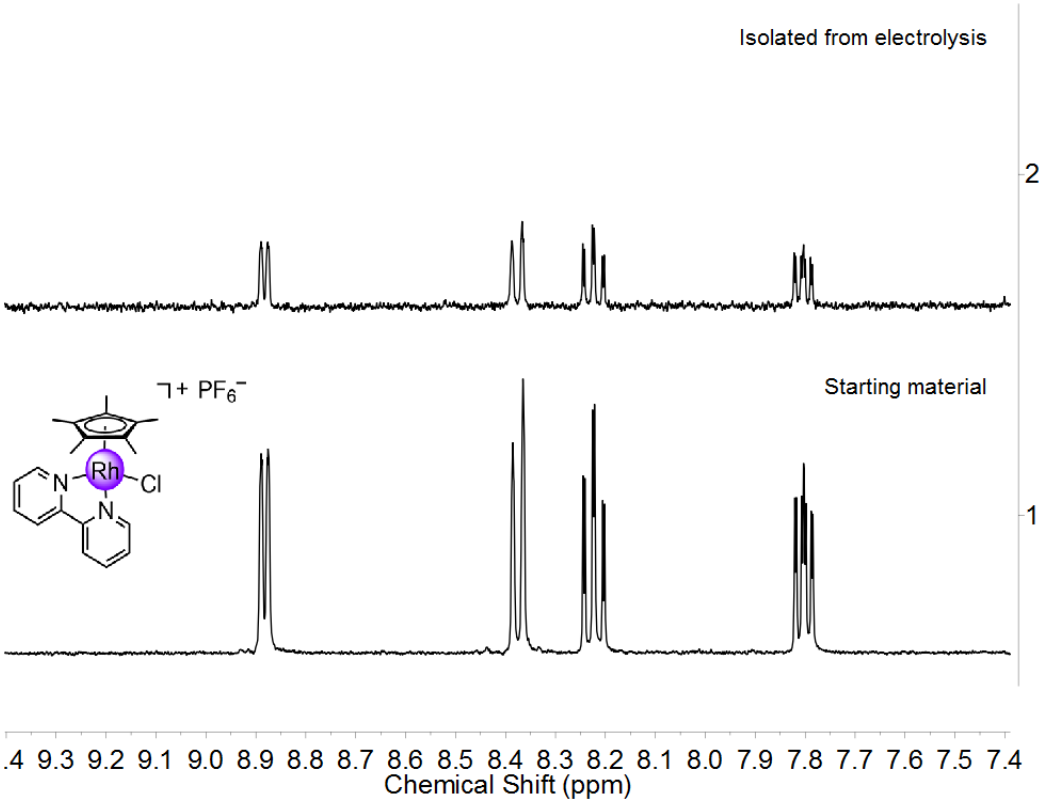

Figure A5: Isolated material from the bulk electrolysis of **2** compared to the starting material.

X-ray Structural Data

Table A1: Crystal data and structure refinement for **[Cp*Rh(tBu-bpy)Cl]$^{+}$PF$_6^{-}$**.

Identification code	k51k
Empirical formula	$C_{29.01}H_{39.48}N_2F_6PCl_{3.02}Rh$
Formula weight	771.37
Temperature/K	225.15
Crystal system	tetragonal
Space group	I4/m
a/Å	22.953(3)
b/Å	22.953(3)
c/Å	13.6618(16)
α/°	90
β/°	90
γ/°	90
Volume/Å^3	7197.5(19)
Z	8
ρ_{calc}g/cm^3	1.424
μ/mm^{-1}	0.796
F(000)	3144.0
Crystal size/mm^3	0.35 × 0.34 × 0.27
Radiation	MoKα (λ = 0.71073)
2Θ range for data collection/°	3.47 to 56.654
Index ranges	$-30 \leq h \leq 30$, $-30 \leq k \leq 30$, $-14 \leq l \leq 18$
Reflections collected	32828
Independent reflections	4678 [R_{int} = 0.0608, R_{sigma} = 0.0372]
Data/restraints/parameters	4678/0/212
Goodness-of-fit on F^2	1.110
Final R indexes [I>=2σ (I)]	R_1 = 0.0764, wR_2 = 0.1947
Final R indexes [all data]	R_1 = 0.1151, wR_2 = 0.2260
Largest diff. peak/hole / e Å^{-3}	1.51/-0.48

Table A2: Bond Lengths for $[Cp^*Rh(tBu\text{-}bpy)Cl]^+PF_6^-$.

Atom	Atom	Length/Å	Atom	Atom	Length/Å
Rh	Cl	2.380(2)	C8	C8[1]	1.414(14)
Rh	N1	2.102(5)	C8	C5AA	1.517(11)
Rh	N1[1]	2.102(5)	C5	C5[1]	1.474(10)
Rh	C7	2.151(6)	C5	C4	1.385(8)
Rh	C7[1]	2.151(6)	C4	C3	1.399(8)
Rh	C6	2.191(8)	C3	C2	1.383(8)
Rh	C8	2.146(6)	C3	C12	1.522(9)
Rh	C8[1]	2.146(6)	C2	C1	1.363(8)
P	F1	1.508(7)	C12	C15	1.522(16)
P	F1[1]	1.508(7)	C12	C14	1.532(14)
P	F2	1.573(7)	C12	C13	1.484(11)
P	F2[1]	1.573(7)	Cl1S	C1S	1.621(11)
P	F3	1.547(10)	C1S	Cl1S[1]	1.621(11)
P	F4	1.529(9)	Cl2S	Cl2S[2]	1.92(2)
N1	C5	1.341(7)	Cl2S	Cl2S[3]	1.92(2)
N1	C1	1.341(7)	Cl2S	C2S[4]	1.79(12)
C7	C6	1.427(9)	Cl2S	C2S	1.79(12)
C7	C10	1.507(10)	C2S	Cl2S[4]	1.79(12)
C7	C8	1.425(10)	C2S	Cl2S[3]	1.79(12)
C6	C7[1]	1.427(9)	C2S	Cl2S[2]	1.79(12)
C6	C9	1.470(15)			

[1]+X,+Y,-Z; [2]+Y,-X,-Z; [3]-Y,+X,+Z; [4]-X,-Y,-Z

Table A3: Bond Angles for $[Cp^*Rh(tBu\text{-}bpy)Cl]^+PF_6^-$.

Atom	Atom	Atom	Angle/°	Atom	Atom	Atom	Angle/°
N1	Rh	Cl	85.28(14)	C6	C7	Rh	72.3(4)
N1[1]	Rh	Cl	85.28(14)	C6	C7	C10	123.9(7)
N1[1]	Rh	N1	76.6(2)	C10	C7	Rh	128.2(5)
N1[1]	Rh	C7[1]	107.6(2)	C8	C7	Rh	70.4(4)
N1	Rh	C7	107.6(2)	C8	C7	C6	108.8(6)
N1	Rh	C7[1]	164.1(2)	C8	C7	C10	127.0(8)
N1[1]	Rh	C7	164.1(2)	C7	C6	Rh	69.3(4)
N1	Rh	C6	141.53(12)	C7[1]	C6	Rh	69.3(4)
N1[1]	Rh	C6	141.53(12)	C7	C6	C7[1]	106.7(8)
N1[1]	Rh	C8	126.0(2)	C7	C6	C9	126.6(4)
N1	Rh	C8[1]	126.0(2)	C7[1]	C6	C9	126.6(4)
N1	Rh	C8	100.4(2)	C9	C6	Rh	124.0(8)
N1[1]	Rh	C8[1]	100.4(2)	C7	C8	Rh	70.8(4)
C7	Rh	Cl	110.1(2)	C7	C8	C5AA	125.5(7)
C7[1]	Rh	Cl	110.1(2)	C8[1]	C8	Rh	70.77(19)
C7[1]	Rh	C7	64.3(4)	C8[1]	C8	C7	107.9(4)
C7[1]	Rh	C6	38.4(2)	C8[1]	C8	C5AA	126.6(5)
C7	Rh	C6	38.4(2)	C5AA	C8	Rh	126.4(5)
C6	Rh	Cl	91.8(2)	N1	C5	C5[1]	114.9(3)
C8[1]	Rh	Cl	148.7(2)	N1	C5	C4	121.3(5)
C8	Rh	Cl	148.7(2)	C4	C5	C5[1]	123.7(3)
C8[1]	Rh	C7[1]	38.7(3)	C5	C4	C3	120.6(5)
C8[1]	Rh	C7	64.5(3)	C4	C3	C12	120.2(6)
C8	Rh	C7[1]	64.5(3)	C2	C3	C4	116.3(6)
C8	Rh	C7	38.7(3)	C2	C3	C12	123.6(6)
C8[1]	Rh	C6	64.6(3)	C1	C2	C3	120.7(5)
C8	Rh	C6	64.6(3)	N1	C1	C2	122.7(5)
C8[1]	Rh	C8	38.5(4)	C3	C12	C14	109.7(7)
F1	P	F1[1]	91.4(9)	C15	C12	C3	109.6(8)
F1[1]	P	F2	177.5(7)	C15	C12	C14	107.2(9)
F1[1]	P	F2[1]	89.8(5)	C13	C12	C3	111.2(7)
F1	P	F2	89.8(5)	C13	C12	C15	108.2(11)
F1	P	F2[1]	177.5(7)	C13	C12	C14	110.8(10)
F1[1]	P	F3	95.4(5)	Cl1S	C1S	Cl1S[1]	118.4(13)
F1	P	F3	95.4(5)	Cl2S[2]	Cl2S	Cl2S[3]	89.997(2)
F1[1]	P	F4	88.7(6)	C2S[4]	Cl2S	Cl2S[3]	58(2)

F1	P	F4	88.7(6)	C2S[4]	Cl2S	Cl2S[2]	58(2)
F2[1]	P	F2	88.9(7)	C2S	Cl2S	Cl2S[2]	58(2)
F3	P	F2	86.7(4)	C2S	Cl2S	Cl2S[3]	58(2)
F3	P	F2[1]	86.7(4)	C2S[4]	Cl2S	C2S	82(9)
F4	P	F2	89.1(5)	Cl2S[2]	C2S	Cl2S	65(5)
F4	P	F2[1]	89.1(5)	Cl2S[3]	C2S	Cl2S	65(5)
F4	P	F3	174.1(8)	Cl2S[3]	C2S	Cl2S[2]	98(9)
C5	N1	Rh	116.3(3)	Cl2S[4]	C2S	Cl2S[2]	65(5)
C5	N1	C1	118.4(5)	Cl2S[3]	C2S	Cl2S[4]	65(5)
C1	N1	Rh	124.9(4)	Cl2S[4]	C2S	Cl2S	98(9)

[1]+X,+Y,-Z; [2]+Y,-X,-Z; [3]-Y,+X,+Z; [4]-X,-Y,-Z

INDEX